

$\Lambda_b \rightarrow \Lambda$ Form Factors from Light-Cone Sum Rules with Λ -Baryon Distribution Amplitudes

F. Mahmoudi^{1,2,3*}, D. Mishra^{1†}

¹*Université Claude Bernard Lyon 1, CNRS/IN2P3,
Institut de Physique des 2 Infinis de Lyon, UMR 5822, F-69622, Villeurbanne, France*

²*Theoretical Physics Department, CERN, CH-1211 Geneva 23, Switzerland*

³*Institut Universitaire de France (IUF), 75005 Paris, France*

Abstract

We compute the $\Lambda_b \rightarrow \Lambda$ transition form factors using light-cone sum rules based on Λ -baryon distribution amplitudes, including contributions up to twist-6. The analysis is performed for pseudoscalar, vector, and axial-vector $b \rightarrow s$ currents and for different choices of the Λ_b interpolating current. We find that only the pseudoscalar interpolating current leads to numerically stable and phenomenologically viable form factors. The resulting form factors are parametrised using a z -expansion and applied to the rare decay $\Lambda_b \rightarrow \Lambda \ell^+ \ell^-$, yielding predictions for branching ratios in the low- q^2 region.

*Electronic address: nazila@cern.ch

†Electronic address: d.mishra@ip2i.in2p3.fr

1 Introduction

Rare decays of bottom hadrons induced by the flavour-changing neutral-current (FCNC) transition $b \rightarrow s\ell^+\ell^-$ provide a sensitive probe of the Standard Model (SM) and of possible effects of physics beyond it. Being loop-suppressed in the SM, these processes are particularly sensitive to contributions from heavy degrees of freedom, while at the same time posing a significant theoretical challenge due to the presence of nonperturbative QCD dynamics. Over the past decade, extensive experimental studies of exclusive $b \rightarrow s\ell^+\ell^-$ decays have been performed at the LHC, most notably by the LHCb collaboration, revealing several tensions between theoretical predictions and data in mesonic channels such as $B \rightarrow K^{(*)}\ell^+\ell^-$ and $B_s \rightarrow \phi\ell^+\ell^-$ (see [1] for a recent analysis).

In this context, baryonic decays of the type $\Lambda_b \rightarrow \Lambda\ell^+\ell^-$ offer a complementary laboratory for testing the flavour sector [2–17]. In contrast to mesonic modes, baryonic transitions provide access to a richer set of angular observables and helicity structures [18–24], and a complementary new physics sensitivity (see e.g. [25–40]). With the increasing precision of measurements [4, 6, 8] in the baryonic sector, a reliable theoretical determination of the hadronic form factors governing the $\Lambda_b \rightarrow \Lambda$ transition has become essential.

The dominant hadronic uncertainties in exclusive $b \rightarrow s\ell^+\ell^-$ decays arise from the form factors. In the low q^2 region, where the final-state hadron carries large energy, light-cone sum rules (LCSR) provide a well-established framework for computing the local form factors in a systematic expansion in terms of hadron distribution amplitudes (DAs). While LCSR methods have been extensively applied to heavy-to-light mesonic transitions, their extension to baryonic decays is technically more involved and remains comparatively less explored (see [3, 16, 41–47]).

In this work, we revisit the determination of the $\Lambda_b \rightarrow \Lambda$ transition form factors using LCSR based on Λ baryon DAs. We include systematically all three-quark Λ DAs up to twist-6 and consider pseudoscalar, vector, and axial-vector $b \rightarrow s$ transition currents. A central aspect of our analysis is a detailed comparison of different interpolating currents for the Λ_b baryon. We explicitly include the contribution of the negative-parity Λ_b^* state in the hadronic representation. Following the strategies previously developed in the context of $\Lambda_b \rightarrow N$ transition [43, 48], we construct suitable linear combinations of invariant amplitudes that eliminate Λ_b^* pole contribution at the level of the sum rules.

We find that, while formally consistent sum rules can be derived for all interpolating currents considered, their numerical behaviour is different. In particular, the pseudoscalar interpolating current leads to form factors that exhibit stable Borel behaviour and satisfy the expected equation-of-motion (EOM) relations and heavy-quark symmetry constraints at leading order, whereas the axial-vector and Ioffe-type currents show reduced stability and weaker consistency within the present framework. Based on this analysis, we identify the pseudoscalar current as providing the most reliable determination of the $\Lambda_b \rightarrow \Lambda$ form factors in LCSR at leading order.

The resulting form factors are transformed into the helicity basis and parametrised using a truncated z -expansion, allowing for a controlled extrapolation in q^2 and a comparison with lattice-QCD results. As an illustration of their phenomenological impact, we apply our form factors to the rare decay $\Lambda_b \rightarrow \Lambda\ell^+\ell^-$ and present predictions for the differential decay rate in the low q^2 region, where the LCSR approach is valid.

The paper is organised as follows. In Sec. 3, we introduce the correlation functions and their hadronic representations. Sec. 3 describes the light-cone operator product expansion (OPE) and the construction of the dispersion relations. The resulting sum rules for the $\Lambda_b \rightarrow \Lambda$ form factors are presented in Sec. 4. Sec. 5 contains the numerical analysis, the comparison of interpolating currents, and the phenomenological application to $\Lambda_b \rightarrow \Lambda\ell^+\ell^-$. We summarise

our findings in Sec. 6. Technical details are collected in the appendices.

2 Correlation function and hadronic representation

The starting point of the light-cone sum-rule analysis of the $\Lambda_b \rightarrow \Lambda$ transition form factors is the following vacuum-to- Λ correlation function:

$$F_i^{(l)}(p, q) = i \int d^4x e^{iq \cdot x} \langle 0 | T \left\{ \eta_{\Lambda_b}^{(l)}(0), j_i(x) \right\} | \Lambda(p) \rangle, \quad (1)$$

where $\eta_{\Lambda_b}^{(l)}$ interpolates the Λ_b baryon, j_i is the $b \rightarrow s$ weak transition current, and the momentum in the Λ_b channel is $p_{\Lambda_b} = p - q$, which defines the variable of the hadronic dispersion relation.

The weak transition currents are chosen as:

$$j_i(x) = \bar{s}(x) \Gamma_i b(x), \quad (2)$$

with¹

$$\Gamma_i \in \{m_b i\gamma_5, \gamma_\mu, \gamma_\mu\gamma_5\}. \quad (3)$$

Here, we neglect m_s in the overall normalisation of the pseudoscalar current.

A central ingredient of the LCSR construction is the choice of the interpolating current for Λ_b baryon, since it governs the coupling to the physical ground state and the pattern of the contributions from excited states. Several local baryonic currents have been considered in the previous analysis [3, 41, 45, 48]; however, not all of them provide a sufficiently strong or clean overlap with the Λ_b ground state in the sum-rule framework.

The Λ_b baryon contains a light diquark system with isospin zero, which restricts the admissible Dirac structures of the interpolating current. In particular, currents built from vector or tensor light-diquark configurations either do not couple to the Λ_b ground state or predominantly excite negative-parity states, leading to a suppressed or contaminated ground-state contribution. As discussed in detail in [43, 49–51], such currents are therefore disfavored in practical LCSR applications.

Guided by the above considerations, we restrict ourselves to interpolating currents that are known to couple to the Λ_b ground state and have been employed in sum-rule analysis. In the present work, we consider three such choices for the Λ_b interpolating current: pseudoscalar, axial-vector, and Ioffe-type currents, defined as:

$$\begin{aligned} \eta^{(\mathcal{P})} &= \epsilon^{abc} (u_a C \gamma_5 d_b) b_c, \\ \eta^{(\mathcal{A})} &= \epsilon^{abc} (u_a C \gamma_5 \gamma_\lambda d_b) \gamma^\lambda b_c, \\ \eta^{(\mathcal{I})} &= \epsilon^{abc} (u_a C \gamma_\lambda d_b) \gamma^\lambda \gamma_5 b_c, \end{aligned} \quad (4)$$

where a, b, c are colour indices and C denotes the charge-conjugation matrix. All three currents carry the quantum numbers of the Λ_b baryon, but differ in their Dirac structures and coupling patterns to the ground and excited states.

The corresponding correlation functions $F_i^{(l)}$ are labeled by the choice of interpolating current,

$$F_i^{(\mathcal{P})} = \{F_5^{(\mathcal{P})}, F_\mu^{(\mathcal{P})}, F_{\mu 5}^{(\mathcal{P})}\}, \quad F_i^{(\mathcal{A})} = \{F_5^{(\mathcal{A})}, F_\mu^{(\mathcal{A})}, F_{\mu 5}^{(\mathcal{A})}\}, \quad F_i^{(\mathcal{I})} = \{F_5^{(\mathcal{I})}, F_\mu^{(\mathcal{I})}, F_{\mu 5}^{(\mathcal{I})}\}. \quad (5)$$

¹In this work we do not consider the tensor weak current $\bar{s} \sigma_{\mu\nu}(\gamma_5) b$. Including tensor currents would require an independent set of correlation functions and tensor form factors, which are beyond the scope of the present analysis.

This classification allows for a systematic comparison of the resulting sum rules and their numerical behaviour for different choices of the interpolating current.

We now proceed to the hadronic representation of the correlation function by inserting a complete set of intermediate states with the quantum numbers of the Λ_b baryon between the interpolating current $\eta_{\Lambda_b}^{(l)}$ and the weak transition current. As a result, the correlation function admits a dispersion representation in the variable $(p - q)^2$, whose lowest-lying contributions arise from the Λ_b ground state and its negative-parity excitation, denoted by Λ_b^* .

The pole contribution of the Λ_b ground state to the hadronic representations determined by two matrix elements. The first one describes the overlap between the vacuum and the Λ_b interpolating current,

$$\langle 0 | \eta_{\Lambda_b}^{(l)} | \Lambda_b(p - q) \rangle = m_{\Lambda_b} f_{\Lambda_b}^{(l)} u_{\Lambda_b}(p - q), \quad (6)$$

where $f_{\Lambda_b}^{(l)}$ denotes the decay constant corresponding to the interpolating current $\eta_{\Lambda_b}^{(l)}$, and $u_{\Lambda_b}(p - q)$ is the Dirac spinor of the Λ_b baryon with momentum $p - q$. The second matrix element encodes the weak transition between the intermediate Λ_b state and the external Λ baryon, $\langle \Lambda(p) | j_i | \Lambda_b(p - q) \rangle$, and is parametrised in terms of $\Lambda_b \rightarrow \Lambda$ form factors. Since the correlation function is analytic in q^2 , the same form factors appear irrespective of whether the transition matrix element is written in the $\Lambda_b \rightarrow \Lambda$ or $\Lambda \rightarrow \Lambda_b$ channel, up to an overall phase that is irrelevant for the present analysis.

For the pseudoscalar weak transition current, the hadronic matrix element is parameterised in terms of a single form factor as:

$$\langle \Lambda(p) | m_b \bar{s} i\gamma_5 b | \Lambda_b(p - q) \rangle = (m_{\Lambda_b} + m_\Lambda) G(q^2) \bar{u}_\Lambda(p) i\gamma_5 u_{\Lambda_b}(p - q), \quad (7)$$

where $G(q^2)$ is a dimensionless form factor.

For the vector and axial-vector weak transition currents, the hadronic matrix elements are parametrised in terms of three independent form factors each. Explicitly, for the vector current one has:

$$\langle \Lambda(p) | \bar{s} \gamma_\mu b | \Lambda_b(p - q) \rangle = \bar{u}_\Lambda(p) \left[f_1(q^2) \gamma_\mu + i \frac{f_2(q^2)}{m_{\Lambda_b}} \sigma_{\mu\nu} q^\nu + \frac{f_3(q^2)}{m_{\Lambda_b}} q_\mu \right] u_{\Lambda_b}(p - q), \quad (8)$$

while for the axial-vector current the corresponding decomposition reads:

$$\langle \Lambda(p) | \bar{s} \gamma_\mu \gamma_5 b | \Lambda_b(p - q) \rangle = \bar{u}_\Lambda(p) \left[g_1(q^2) \gamma_\mu + i \frac{g_2(q^2)}{m_{\Lambda_b}} \sigma_{\mu\nu} q^\nu + \frac{g_3(q^2)}{m_{\Lambda_b}} q_\mu \right] \gamma_5 u_{\Lambda_b}(p - q). \quad (9)$$

The form factors $f_i(q^2)$ and $g_i(q^2)$ encode the nonperturbative QCD dynamics of the $\Lambda_b \rightarrow \Lambda$ transition and constitute the central hadronic inputs for the description of rare and semileptonic Λ_b decays. Their reliable determination is therefore essential for precision phenomenology in the heavy-baryon sector.

Although the Λ_b ground-state provides the leading contribution to the hadronic dispersion relation, the relatively small mass gap between the Λ_b and its lowest negative-parity excitation Λ_b^* implies that the latter can give a non-negligible contribution in the sum-rule analysis. It is therefore natural to include the Λ_b^* pole explicitly in the hadronic representation of the correlation function, in order to achieve a more complete and controlled description of the intermediate-state contributions.

The contribution of the negative-parity Λ_b^* state to the hadronic representation is described by the residue of its pole, which factorises into the product of the corresponding decay constant

and the weak transition matrix element. The coupling of the interpolating current to the Λ_b^* state is defined as:

$$\langle 0 | \eta_{\Lambda_b}^{(l)} | \Lambda_b^*(p - q) \rangle = m_{\Lambda_b^*} f_{\Lambda_b^*}^{(l)} \gamma_5 u_{\Lambda_b^*}(p - q). \quad (10)$$

where $f_{\Lambda_b^*}^{(l)}$ denotes the decay constant associated with the interpolating current $\eta_{\Lambda_b}^{(l)}$, and the explicit γ_5 reflects the opposite parity of the Λ_b^* state relative to the ground-state Λ_b baryon. The above matrix element is combined with the weak transition matrix element $\langle \Lambda(p) | j_i | \Lambda_b^*(p - q) \rangle$, which can be parametrised in terms of independent form factors in close analogy to the $\Lambda_b \rightarrow \Lambda$ case.

As an explicit example, for the pseudoscalar transition current one obtains:

$$\langle \Lambda(p) | m_b \bar{s} i\gamma_5 b | \Lambda_b^*(p - q) \rangle = (m_{\Lambda_b^*} - m_\Lambda) \hat{G}(q^2) \bar{u}_\Lambda(p) i u_{\Lambda_b^*}(p - q), \quad (11)$$

where $\hat{G}(q^2)$ denotes the pseudoscalar form factor associated with the Λ_b^* intermediate state. Analogously, the matrix elements of the vector and axial-vector transition currents between the Λ_b^* and Λ baryons are parameterised in terms of form factors $\hat{f}_{1,2,3}(q^2)$ and $\hat{g}_{1,2,3}(q^2)$, respectively, whose explicit Lorentz decompositions follow the same pattern as in Eqs. (8) and (9), up to the appropriate parity structure.

To complete the construction of the hadronic representation, we decompose the correlation function in Eq. (1) into Lorentz structures, whose coefficient functions depend on the kinematic variables $(p - q)^2$ and q^2 . These invariant amplitudes form the basis for establishing dispersion relations in the Λ_b channel. For the pseudoscalar transition current, the correlation function can be written as:

$$F_5^{(l)}(P, q) = \left[F_1^{(l)}((p - q)^2, q^2) + q \not{F}_2^{(l)}((p - q)^2, q^2) \right] i\gamma_5 u_\Lambda(p), \quad (12)$$

where $l = \mathcal{P}, \mathcal{A}, \mathcal{I}$ labels the choice of the Λ_b interpolating current.

For the vector transition current, the correlation function is parameterised in terms of six independent invariant amplitudes as:

$$F_\mu^{(l)}(p, q) = \left(\tilde{F}_1^{(l)} p_\mu + \tilde{F}_2^{(l)} p_\mu \not{q} + \tilde{F}_3^{(l)} \gamma_\mu + \tilde{F}_4^{(l)} \gamma_\mu \not{q} + \tilde{F}_5^{(l)} q_\mu + \tilde{F}_6^{(l)} q_\mu \not{q} \right) u_\Lambda(p), \quad (13)$$

while for the axial-vector transition current one finds:

$$F_{\mu 5}^{(l)}(P, q) = \left(\bar{F}_1^{(l)} P_\mu + \bar{F}_2^{(l)} P_\mu \not{q} + \bar{F}_3^{(l)} \gamma_\mu + \bar{F}_4^{(l)} \gamma_\mu \not{q} + \bar{F}_5^{(l)} q_\mu + \bar{F}_6^{(l)} q_\mu \not{q} \right) \gamma_5 u_\Lambda(p). \quad (14)$$

Employing the hadronic matrix elements introduced above and summing over the spins of the intermediate Λ_b and Λ_b^* states, one obtains a dispersion relation for the invariant amplitudes in the variable $(p - q)^2$. As an explicit example, for the pseudoscalar transition current, the combined invariant amplitudes $F_{1,2}^{(l)}$ read:

$$\begin{aligned} F_5^{(l)}(P, q) &= \frac{m_{\Lambda_b} f_{\Lambda_b}^{(l)} G(q^2)}{m_{\Lambda_b}^2 - (p - q)^2} \left[(m_{\Lambda_b}^2 - m_\Lambda^2) - (m_{\Lambda_b} + m_\Lambda) \not{q} \right] i\gamma_5 u_\Lambda(p) \\ &+ \frac{m_{\Lambda_b^*} f_{\Lambda_b^*}^{(l)} \hat{G}(q^2)}{m_{\Lambda_b^*}^2 - (p - q)^2} \left[(m_{\Lambda_b^*}^2 - m_\Lambda^2) + (m_{\Lambda_b^*} - m_\Lambda) \not{q} \right] i\gamma_5 u_\Lambda(p) \\ &+ \int_{s_0^h}^{\infty} \frac{ds}{s - (p - q)^2} (\rho_1^{(l)}(s, q^2) + \rho_2^{(l)}(s, q^2) \not{q}) i\gamma_5 u_\Lambda(p), \end{aligned} \quad (15)$$

where $\rho_{1,2}^{(l)}(s, q^2)$ denote the hadronic spectral densities associated with higher resonances and continuum states carrying the quantum numbers of the Λ_b baryon, and s_0^h is the corresponding effective continuum threshold. In the case of vector and axial vector transition currents, an analogous dispersion representation arises for each of the six invariant amplitudes defined in Eqs. (13) and (14). For brevity, the explicit expressions for these amplitudes are collected in Appendix A.

3 Light-cone OPE and dispersion relation

We compute the correlation functions defined in Eq. (1) in QCD by performing a light-cone expansion of the time-ordered product of currents at $x^2 \rightarrow 0$. The external kinematics are chosen such that the momentum flowing through the Λ_b channel, $(p - q)^2$, is spacelike and large, ensuring that the correlation function is dominated by light-like distances and can be expressed in terms of Λ -baryon DAs.

Throughout this analysis, we neglect light-quark masses, retaining only the heavy-quark mass m_b and the physical Λ -baryon mass m_Λ , which enters the kinematics and the normalisation of the Λ DAs. At leading order in the strong coupling, the correlation function factorises into perturbatively calculable hard-scattering kernels, arising from the virtual b -quark propagator, convoluted with three-quark Λ DAs. The resulting expression is organised as a sum over contributions of increasing twist. In the present work, we include all three-quark Λ DAs from twist-3 up to twist-6. The explicit definitions of the Λ DAs, together with their normalisation and parameters, are collected in Appendix B.

Substituting the light-cone expansions of the quark-level matrix elements in terms of Λ DAs into the correlation functions $F_5^{(l)}$, $F_\mu^{(l)}$, and $F_{\mu 5}^{(l)}$, one can project out the corresponding invariant amplitudes defined in Eqs. (12)-(14). On the QCD side, these amplitudes are obtained as convolution integrals of the hard-scattering kernels with the Λ DAs and depend on the variables $(p - q)^2$ and q^2 .

Each invariant amplitude admits an independent dispersion representation in the Λ_b channel. For a given choice of interpolating current, the dispersion relations contain pole contributions from the Λ_b and Λ_b^* states, as well as continuum contributions from higher-mass states. In the case of the vector and axial-vector transition currents, six linearly independent invariant amplitudes arise, leading to six corresponding dispersion relations.

The dispersion relations obtained for the individual invariant amplitudes generally receive contributions from both the Λ_b ground state and its negative-parity excitation Λ_b^* . In order to isolate the ground-state contribution, we follow the standard strategy of forming suitable linear combinations of invariant amplitudes such that the Λ_b^* pole cancels identically. This procedure exploits the different parity structure of the Λ_b and Λ_b^* contributions and allows one to construct sum rules that depend only on the Λ_b ground-state matrix elements.

As an explicit example, for the pseudoscalar transition current, an appropriate linear combination of the invariant amplitudes $F_1^{(l)}$ and $F_2^{(l)}$ eliminates the Λ_b^* contribution and leads to the following dispersion relation:

$$\begin{aligned} \frac{m_{\Lambda_b}(m_{\Lambda_b} + m_\Lambda)(m_{\Lambda_b} + m_{\Lambda_b^*})\lambda_{\Lambda_b}^{(l)}G(q^2)}{m_{\Lambda_b}^2 - (p - q)^2} + \int_{s_0^h}^{\infty} ds \frac{\rho_1^{(l)}(s, q^2) - (m_{\Lambda_b^*} + m_\Lambda)\rho_2^{(l)}(s, q^2)}{s - (p - q)^2} \\ = \left[F_1^{(l)}((p - q)^2, q^2) - (m_{\Lambda_b^*} + m_\Lambda)F_2^{(l)}((p - q)^2, q^2) \right]. \end{aligned} \quad (16)$$

The contributions of higher resonances and continuum states in the Λ_b channel are approximated using semi-global quark-hadron duality. Concretely, the continuum contribution appearing in the dispersion relation for the linear combination of invariant amplitudes is replaced by the imaginary part of the corresponding QCD expressions above an effective threshold s_0 ,

$$\int_{s_0^h}^{\infty} ds \frac{\rho_1^{(l)}(s, q^2) - (m_{\Lambda_b^*} + m_{\Lambda})\rho_2^{(l)}(s, q^2)}{s - (p - q)^2} \approx \frac{1}{\pi} \int_{s_0}^{\infty} ds \frac{\text{Im}_s F_1^{(l)}(s, q^2) - (m_{\Lambda_b^*} + m_{\Lambda}) \text{Im}_s F_2^{(l)}(s, q^2)}{s - (p - q)^2}, \quad (17)$$

where s_0 denotes the effective continuum threshold and the spectral densities $\text{Im}_s F_{1,2}^{(l)}$ are obtained from the light-cone OPE.

Employing the decomposition of the Λ -baryon matrix elements in terms of DAs, the invariant amplitudes can be written as convolution integrals over the momentum fractions x_i . After using the δ -function constraint to eliminate one variable and performing one trivial integration, the correlation functions reduce to a single remaining integral,

$$F_j^{(l)} = \frac{m_b}{4} \sum_{n=1}^3 \int_0^1 dx_2 \frac{T_{jn}^{(l)}(x_2, (p - q)^2, q^2)}{\Delta^n}, \quad (18)$$

with $\Delta = m_b^2 - x_2(p - q)^2 + x_2\bar{x}_2 m_{\Lambda}^2 - \bar{x}_2 q^2$.

The integrals can be cast into a dispersion form by introducing the variable:

$$s(x_2) = \frac{m_b^2 - \bar{x}_2 q^2 + x_2 \bar{x}_2 m_{\Lambda}^2}{x_2}, \quad (19)$$

with the inverse transformation:

$$x_2(s) = \frac{1}{2m_{\Lambda}^2} \left[m_{\Lambda}^2 + q^2 - s + \sqrt{(s - q^2 - m_{\Lambda}^2)^2 + 4m_{\Lambda}^2(m_b^2 - q^2)} \right]. \quad (20)$$

The above representation provides the QCD input needed for the construction of light-cone sum rules for the $\Lambda_b \rightarrow \Lambda$ form factors, which is discussed in the next section.

4 Light-cone sum rules for $\Lambda_b \rightarrow \Lambda$ form factors

Combining the light-cone OPE of the correlation functions with their hadronic dispersion representations, and applying quark-hadron duality together with a Borel transformation in the Λ_b channel, we obtain light-cone sum rules for the $\Lambda_b \rightarrow \Lambda$ transition form factors. In this section, we collect the resulting sum rules that serve as the basis for the numerical analysis. The light-cone sum rule for the pseudoscalar form factor is:

$$G(q^2) = \frac{e^{m_{\Lambda_b}^2/M^2}}{m_{\Lambda_b}(m_{\Lambda_b} + m_{\Lambda})(m_{\Lambda_b} + m_{\Lambda}^*)\lambda_{\Lambda_b}^{(l)}} \frac{1}{\pi} \int_{m_b^2}^{s_0} ds e^{-s/M^2} \times \left[\text{Im}_s F_1^{(l)}(s, q^2) - (m_{\Lambda_b^*} + m_{\Lambda}) \text{Im}_s F_2^{(l)}(s, q^2) \right]. \quad (21)$$

For the vector transition current, the LCSR for the form factors $f_1(q^2)$, $f_2(q^2)$, and $f_3(q^2)$ are obtained from the corresponding linear combinations of invariant amplitudes after Borel transformation and continuum subtraction. They read:

$$f_1(q^2) = \frac{e^{m_{\Lambda_b}^2/M^2}}{2m_{\Lambda_b}(m_{\Lambda_b} + m_{\Lambda_b^*})\lambda_{\Lambda_b}^{(l)}} \frac{1}{\pi} \int_{m_b^2}^{s_0} ds e^{-s/M^2} \left[(m_{\Lambda_b} + m_{\Lambda}) \left(\text{Im}_s \tilde{F}_1^{(l)}(s, q^2) \right. \right. \\ \left. \left. - (m_{\Lambda_b^*} - m_{\Lambda}) \text{Im}_s \tilde{F}_2^{(l)}(s, q^2) \right) + 2 \text{Im}_s \tilde{F}_3^{(l)}(s, q^2) + 2(m_{\Lambda_b^*} - m_{\Lambda_b}) \text{Im}_s \tilde{F}_4^{(l)}(s, q^2) \right], \quad (22)$$

$$f_2(q^2) = \frac{e^{m_{\Lambda_b}^2/M^2}}{2(m_{\Lambda_b} + m_{\Lambda_b^*})\lambda_{\Lambda_b}^{(l)}} \frac{1}{\pi} \int_{m_b^2}^{s_0} ds e^{-s/M^2} \left[\text{Im}_s \tilde{F}_1^{(l)}(s, q^2) - (m_{\Lambda_b^*} - m_{\Lambda}) \text{Im}_s \tilde{F}_2^{(l)}(s, q^2) \right. \\ \left. - 2 \text{Im}_s \tilde{F}_4^{(l)}(s, q^2) \right], \quad (23)$$

and

$$f_3(q^2) = \frac{e^{m_{\Lambda_b}^2/M^2}}{2(m_{\Lambda_b} + m_{\Lambda_b^*})\lambda_{\Lambda_b}^{(l)}} \frac{1}{\pi} \int_{m_b^2}^{s_0} ds e^{-s/M^2} \left[\text{Im}_s \tilde{F}_1^{(l)}(s, q^2) - (m_{\Lambda_b^*} - m_{\Lambda}) (2 \text{Im}_s \tilde{F}_6^{(l)}(s, q^2) \right. \\ \left. + \text{Im}_s \tilde{F}_2^{(l)}(s, q^2)) + 2(\text{Im}_s \tilde{F}_5^{(l)}(s, q^2) + \text{Im}_s \tilde{F}_4^{(l)}(s, q^2)) \right]. \quad (24)$$

The LCSR for the axial-vector form factors $g_1(q^2)$, $g_2(q^2)$, and $g_3(q^2)$ follow analogously from the above expressions by replacing the vector invariant amplitudes $\text{Im}_s \tilde{F}_j^{(l)}$ with their axial-vector counterparts $\text{Im}_s \bar{F}_j^{(l)}$ and reversing the sign of the Λ -baryon mass, $m_{\Lambda} \rightarrow -m_{\Lambda}$.

In practice, the transformation of the light-cone expressions into dispersion integrals, the subtraction of continuum contributions, and the Borel transformation in the Λ_b channel can be implemented simultaneously through a set of universal substitution rules. For integrals of the type appearing in Eq. (1), one makes the replacements:

$$\int dx \frac{T(x)}{\Delta} \rightarrow \int_{x_0}^1 \frac{dx}{x} T(x) \exp \left(-\frac{s(x)}{M^2} \right), \\ \int dx \frac{T(x)}{\Delta^2} \rightarrow \frac{1}{M^2} \int_{x_0}^1 \frac{dx}{x^2} T(x) \exp \left(-\frac{s(x)}{M^2} \right) + \frac{T(x_0) e^{-s_0/M^2}}{m_b^2 + x_0^2 m_{\Lambda}^2 - q^2}, \\ \int dx \frac{T(x)}{\Delta^3} \rightarrow \frac{1}{2M^4} \int_{x_0}^1 \frac{dx}{x^3} T(x) \exp \left(-\frac{s(x)}{M^2} \right) + \frac{1}{2M^2} \frac{T(x_0) e^{-s_0/M^2}}{x_0 (m_b^2 + x_0^2 m_{\Lambda}^2 - q^2)} \\ - \frac{1}{2} \frac{x_0^2 e^{-s_0/M^2}}{(m_b^2 + x_0^2 m_{\Lambda}^2 - q^2)} \frac{d}{dx} \left(\frac{T(x)}{x (m_b^2 + x^2 m_{\Lambda}^2 - q^2)} \right) \Big|_{x=x_0}. \quad (25)$$

Parameter	Value(s)	Reference(s)
f_Λ	$(6.0 \pm 0.3) \times 10^{-3} \text{ GeV}^2$	[53]
λ_1	$(1.0 \pm 0.3) \times 10^{-2} \text{ GeV}^2$	[53]
λ_2	$(0.83 \pm 0.05) \times 10^{-2} \text{ GeV}^2$	[53]
λ_3	$(0.83 \pm 0.05) \times 10^{-2} \text{ GeV}^2$	[53]
m_Λ	1.115 GeV	[52]
m_{Λ_b}	5.620 GeV	[52]
$m_{\Lambda_b^*}$	5.850 GeV	[52]
$\lambda_{\Lambda_b}^P$	$(0.0109 \pm 0.0031) \text{ GeV}$	[43]
$\lambda_{\Lambda_b}^A$	$(0.0127 \pm 0.0034) \text{ GeV}$	[43]
$\lambda_{\Lambda_b}^T$	$(0.022 \pm 0.0049) \text{ GeV}$	[43]
M^2	$(20 \pm 5) \text{ GeV}^2$	[see text]
s_0	$40 \pm 1 \text{ GeV}^2$	[see text]

Table 1: Overview of the input parameters used in this study.

Here $x_0 \equiv x(s_0)$ denotes the solution of $s(x_0) = s_0$, and $T(x)$ represents a generic numerator function arising from the convolution of hard-scattering kernels with Λ DAs. The surface terms appearing on the right-hand side originate from the conversion of higher-power denominators, Δ^{-n} with $n = 2, 3$, into the canonical dispersion form with a single pole in $s - (p - q)^2$.

5 Numerical Analysis

We begin by specifying the numerical values of input parameters entering the LCSR. The parameters of the Λ -baryon DAs are taken from QCD sum-rule analyses and are summarised in Table 1. The explicit definitions and conventions for the Λ DAs are collected in Appendix A. The baryon masses are taken from the Particle Data Group [52]. For the heavy-quark mass entering the correlation functions, we employ the $\overline{\text{MS}}$ mass scheme. In particular, we use $\bar{m}_b(\bar{m}_b) = 4.16 \pm 0.03 \text{ GeV}$ [54]. Since perturbative $\mathcal{O}(\alpha_s)$ corrections are not included in the present analysis, the only scale dependence arises from the factorisation scale μ_f associated with the Λ DAs. We adopt $\mu_f = \mu_b = 4.0 \pm 1.0 \text{ GeV}$.

Instead of inserting fixed numerical values for the Λ_b decay constants into the sum rules, we consistently employ the corresponding two-point QCD sum rules for each choice of interpolating current, following the strategy advocated in Ref. [43]. This procedure reduces the sensitivity to the decay-constant normalisation and partially cancels systematic uncertainties.

We now specify the choice of the Borel parameter M^2 and the effective continuum threshold s_0 entering the light-cone sum rules. As a consistency check of the numerical analysis, the working window for M^2 is chosen such that higher-twist contributions are adequately suppressed at small M^2 , while continuum contributions remain under control at larger values. The threshold parameter s_0 is fixed by requiring that the corresponding daughter sum rules reproduce

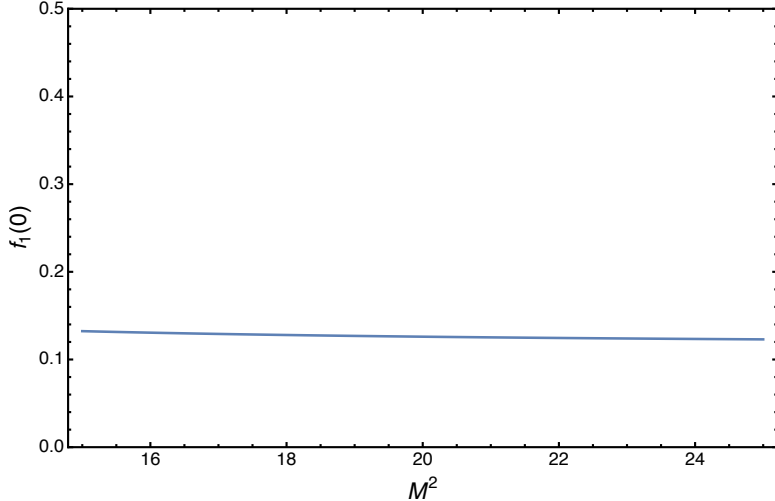


Figure 1: Borel-parameter dependence of the form factor $f_1(q^2)$ at fixed q^2 for the pseudoscalar interpolating current. The shaded band indicates the selected Borel window.

Form factor	$\eta^{(\mathcal{P})}$	$\eta^{(\mathcal{A})}$	$\eta^{(\mathcal{I})}$
$G(0)$	$0.085^{+0.035}_{-0.021}$	$0.023^{+0.014}_{-0.011}$	$-0.099^{+0.017}_{-0.025}$
$f_1(0)$	$0.096^{+0.041}_{-0.023}$	$0.046^{+0.018}_{-0.009}$	$0.105^{+0.031}_{-0.020}$
$f_2(0)$	$-0.034^{+0.008}_{-0.015}$	$0.023^{+0.009}_{-0.006}$	$0.083^{+0.025}_{-0.015}$
$g_1(0)$	$0.094^{+0.040}_{-0.023}$	$0.053^{+0.021}_{-0.011}$	$-0.058^{+0.012}_{-0.019}$
$g_2(0)$	$-0.014^{+0.003}_{-0.006}$	$-0.062^{+0.013}_{-0.024}$	$-0.006^{+0.006}_{-0.007}$

Table 2: Numerical results of $\Lambda_b \rightarrow \Lambda$ transition Form factors at zero squared momentum transfer. It is obtained within LCSR framework with different interpolating currents.

the physical Λ_b mass within a reasonable accuracy. Within these choices, the extracted form factors exhibit a stable behaviour with respect to variations of M^2 , as illustrated in Fig. 1 for the representative case of $f_1(q^2)$ obtained with the pseudoscalar interpolating current. Similar stability behaviour is observed for the remaining form factors. The numerical values adopted for M^2 and s_0 are summarised in Table 1.

In order to assess the sensitivity of the light-cone sum rules to the choice of the Λ_b interpolating current, we compute the $\Lambda_b \rightarrow \Lambda$ form factors using three commonly employed currents: the pseudoscalar, axial-vector, and Ioffe currents. For each choice, the sum rules are evaluated using the corresponding decay constants obtained from two-point QCD sum rules, as discussed in the previous subsection. Table 2 summarises the numerical values of the form factors at a fixed momentum transfer for the three interpolating currents. Although, in principle, different interpolating currents for the Λ_b baryon can be employed to construct light-cone sum rules, we find that the axial-vector and Ioffe interpolating currents lead to numerically less reliable results in the present analysis. In particular, the form factors extracted from these currents do not satisfy the QCD equation-of-motion relations linking pseudoscalar and axial-vector matrix elements within uncertainties. This signals an incomplete numerical cancellation of unphysical contributions in the corresponding sum rules. In contrast, the pseudoscalar interpolating current leads to stable sum rules, exhibits good convergence in the chosen Borel window, and

yields form factors that are consistent with EOM constraints. For these reasons, only the form factors obtained from the pseudoscalar interpolating current ensure maximal theoretical control and provide results that are compatible with known phenomenological constraints.

Although radiative corrections are neglected in this work, the qualitative conclusions concerning the choice of interpolating current are expected to remain unchanged. The relative performance of the pseudoscalar, axial-vector, and Ioffe currents is mainly governed by their overlap with the Λ_b ground state and their sensitivity to negative-parity excitations and higher-twist contributions, which are fixed by their Dirac structure. Existing studies of $\mathcal{O}(\alpha_s)$ corrections within soft-collinear effective theory (SCET) [46, 55] indicate that radiative effects primarily affect normalisation rather than the underlying structure of the sum rules. A complete calculation of radiative corrections within the full QCD light-cone sum-rule framework is beyond the scope of the present work and is left for future studies.

As an additional validation of our implementation, we consider the proton limit of the present framework. Replacing the Λ baryon by the proton and employing the corresponding proton DAs, we reproduce the light-cone sum-rule results for nucleon form factors obtained in Ref. [43]. This provides a non-trivial cross-check of the analytical expressions, the numerical implementation of the light-cone expansion, and the treatment of the dispersion relations.

The light-cone sum rules derived in Sec. 4 provide the form factors in terms of the invariant amplitudes $f_{1,2,3}(q^2)$ and $g_{1,2,3}(q^2)$. For phenomenological applications and for a direct comparison with lattice-QCD results, it is convenient to express these form factors in an alternative basis. Following standard conventions [56], we therefore transform our results to the helicity form-factor basis $\{f_+(q^2), f_\perp(q^2), g_+(q^2), g_\perp(q^2)\}$. The relations between the two bases [55] are given by:

$$f_+(q^2) = f_1(q^2) - \frac{q^2}{m_{\Lambda_b}(m_{\Lambda_b} + m_\Lambda)} f_2(q^2), \quad (26)$$

$$f_\perp(q^2) = f_1(q^2) - \frac{(m_{\Lambda_b} + m_\Lambda)}{m_{\Lambda_b}} f_2(q^2), \quad (27)$$

$$g_+(q^2) = g_1(q^2) + \frac{q^2}{m_{\Lambda_b}(m_{\Lambda_b} - m_\Lambda)} g_2(q^2), \quad (28)$$

$$g_\perp(q^2) = g_1(q^2) + \frac{(m_{\Lambda_b} - m_\Lambda)}{m_{\Lambda_b}} g_2(q^2), \quad (29)$$

where contributions proportional to $f_3(q^2)$ and $g_3(q^2)$ do not enter the helicity form factors for massless leptons.

In Fig. 2, we present the numerical results for the helicity form factors obtained from light-cone sum rules using the pseudoscalar interpolating current. The form factors are shown in the low- q^2 region where the LCSR approach is expected to be reliable, and the shaded bands represent the total uncertainties estimated from the sum-rule analysis. In order to extrapolate the light-cone sum-rule results beyond the low- q^2 region and to facilitate phenomenological applications, we parametrise the helicity form factors $F \in \{f_+, g_+, f_\perp, g_\perp\}$ using a truncated z -expansion [57]. For each form factor, we adopt a parametrisation including a single pole factor accounting for the nearest B_s -like resonance,

$$F(q^2) = \frac{1}{1 - q^2/M_F^2} \sum_{n=0}^K a_n^{(F)} z(q^2)^n, \quad z(q^2) = \frac{\sqrt{t_+ - q^2} - \sqrt{t_+ - t_0}}{\sqrt{t_+ - q^2} + \sqrt{t_+ - t_0}}, \quad (30)$$

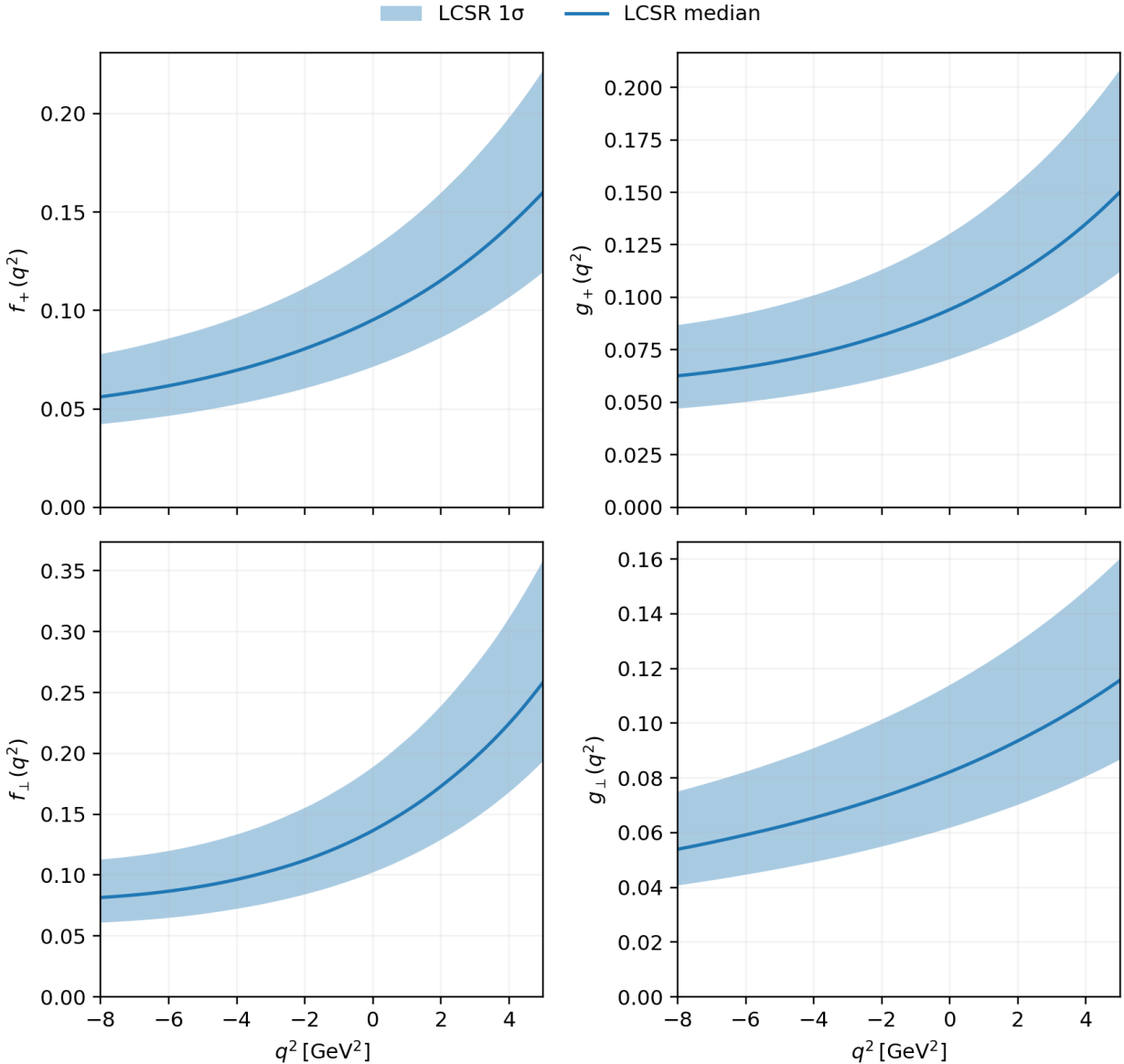


Figure 2: Helicity form factors for the $\Lambda_b \rightarrow \Lambda$ transition obtained from light-cone sum rules using the pseudoscalar interpolating current. The solid lines denote the median values, while the shaded bands represent the total LCSR uncertainties.

where $t_0 = (m_{\Lambda_b} - m_\Lambda)^2$ and $t_+ = (m_B + m_K)^2$.

The pole masses are chosen as $M_{f_+} = M_{f_\perp} = 5.416$ GeV and $M_{g_+} = M_{g_\perp} = 5.750$ GeV, following the conventions adopted in lattice-QCD analyses [56]. The coefficients $a_n^{(F)}$ are determined by fitting the z -expanded form factors to the LCSR results shown in Fig. 2. In the numerical analysis, we truncate the expansion at $K = 2$, which is sufficient to describe the LCSR data within uncertainties. The resulting fit parameters are collected in Table 3. The full correlation matrices of the z -expansion coefficients are provided as ancillary file. The uncertainties are determined through a Monte Carlo sampling of all input parameters, that are listed in Table 1. For each sampled parameter set, the complete LCSR is evaluated, generating a distribution of form-factor values at fixed q^2 . The central value is defined as the median of this distribution, and the associated uncertainty is obtained from the central 68% probability

Form factor	a_0	a_1	a_2
f_+	0.620 ± 0.320	-3.635 ± 1.879	6.093 ± 3.150
f_\perp	1.408 ± 0.727	-9.349 ± 4.835	10.892 ± 8.743
g_+	0.434 ± 0.223	-2.323 ± 1.198	3.853 ± 1.988
g_\perp	0.434 ± 0.223	-2.426 ± 1.251	4.082 ± 2.106

Table 3: z -expansion coefficients for the helicity form factors obtained from LCSR fits.

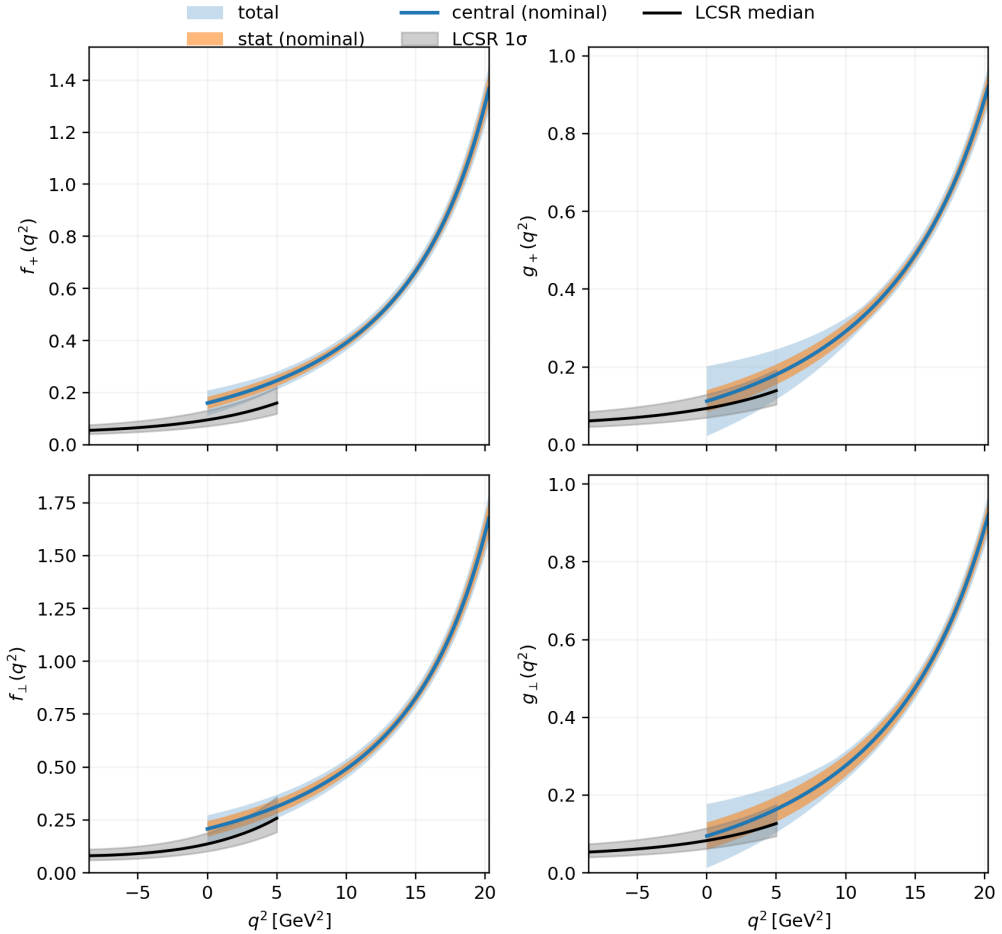


Figure 3: Comparison of helicity form factors $f_+(q^2)$, $g_+(q^2)$, $f_\perp(q^2)$, and $g_\perp(q^2)$ from LCSR (low q^2) and lattice-QCD (high q^2), shown as independent determinations with their respective uncertainty bands. This figure serves as an input-level cross-check prior to the combined fit.

interval. Correlation between different form factors and between different kinematic points are preserved in this procedure and subsequently propagated to the z -expansion fits.

5.1 Combined LCSR and lattice-QCD form factors for $\Lambda_b \rightarrow \Lambda$

In order to obtain a reliable description of the $\Lambda_b \rightarrow \Lambda$ form factors over the full kinematic range, we perform a combined analysis of LCSR results at low momentum transfer and lattice-

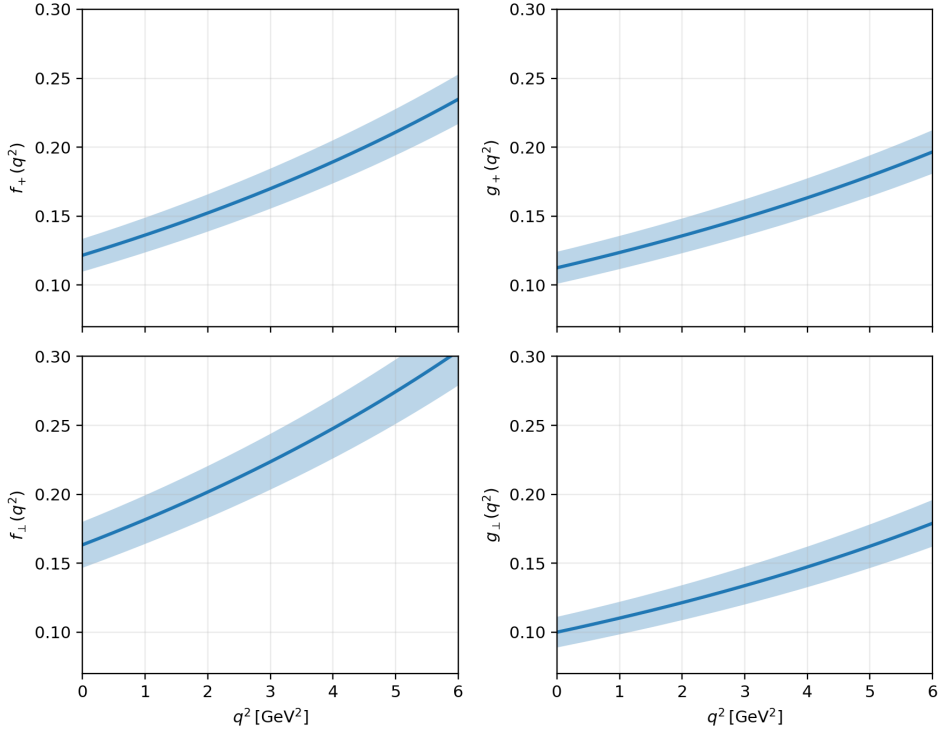


Figure 4: Combined-fit helicity form factors $f_+(q^2)$, $g_+(q^2)$, $f_\perp(q^2)$, and $g_\perp(q^2)$ obtained from the joint LCSR+lattice analysis, shown here in the low- q^2 region. The solid curves denote the fitted central values and the shaded bands represent the total fit uncertainties.

QCD determinations at high q^2 . The two methods are complementary: LCSR is applicable in the large-recoil region, while lattice-QCD provides controlled results near zero recoil.

As an intermediate consistency check, the LCSR and lattice inputs are first compared at the level of individual form factors, showing agreement within uncertainties in the region where their domains approach each other (see Fig. 3). We then construct a unified parametrisation by fitting both datasets simultaneously using the same z -parametrisation as Eq. 30.

Here, the coefficients $a_n^{(F)}$ are determined from a simultaneous fit to LCSR and lattice-QCD input points using a common parametrisation². Specifically, we use four LCSR points at $q^2 = \{-8, -4, -2, 0\} \text{ GeV}^2$ and four lattice-QCD points at $q^2 = \{13, 15, 17, 19\} \text{ GeV}^2$ for each helicity form factor. Unless stated otherwise, we truncate the z -expansion at $K = 2$, which provides a stable description of both datasets within uncertainties. The resulting combined-fit form factors are shown in Fig. 4 for the low- q^2 region $0 \leq q^2 \leq 6 \text{ GeV}^2$.

5.2 Differential branching ratio of $\Lambda_b \rightarrow \Lambda \ell^+ \ell^-$

Having determined the $\Lambda_b \rightarrow \Lambda$ form factors from LCSRs and parametrised their q^2 dependence using the z -expansion, we now turn to their phenomenological implications. In particular, we consider the rare semileptonic decay $\Lambda_b \rightarrow \Lambda \ell^+ \ell^-$ and focus on the dilepton invariant-mass spectrum in the low- q^2 region, where the LCSR approach is expected to provide reliable predictions. The vector and axial-vector helicity form factors entering the decay amplitude

²The coefficients a_n^F and their correlation matrices are provided in ancillary files.

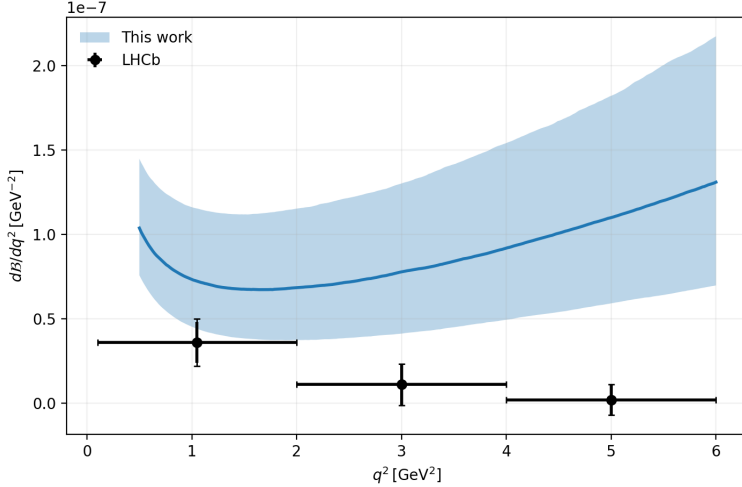


Figure 5: Differential branching fraction $d\mathcal{B}/dq^2$ for the decay $\Lambda_b \rightarrow \Lambda \ell^+ \ell^-$ in the low- q^2 region. The solid line denotes the central value and the shaded band represents the combined theoretical uncertainty.

are taken from the extrapolated LCSR results obtained with the pseudoscalar interpolating current. Since tensor form factors are not computed within the present LCSR framework, their contribution to the branching fraction is incorporated using lattice-QCD results [56]. The resulting prediction for $d\mathcal{B}/dq^2$ is shown in Fig 5. The restriction to the low- q^2 region reflects the domain of the applicability of the light-cone sum-rule method; predictions at higher values of q^2 rely on extrapolated form factors and are therefore not shown here. Compared to the theory prediction of the $\Lambda_b \rightarrow \Lambda \ell^+ \ell^-$ branching ratio based on lattice-QCD form factors as implemented in SuperIso [58–60] are slightly larger.

6 Summary and Discussion

In this work, we have presented a light-cone sum-rule analysis of the $\Lambda_b \rightarrow \Lambda$ transition form factors induced by pseudoscalar, vector, and axial-vector $b \rightarrow s$ currents. The calculation is based on vacuum-to- Λ correlation functions, evaluated using a light-cone OPE in terms of three-quark Λ -baryon DAs. All contributions from twist-3 up to twist-6 DAs have been consistently included. The resulting sum rules are valid at leading order in the strong coupling and provide a systematic framework for studying heavy-to-light baryonic transitions at low momentum transfer, while radiative α_s corrections are left for future study.

A central aspect of our analysis is the careful treatment of the Λ_b interpolating current. We have investigated three commonly used choices –the pseudoscalar, axial-vector, and Ioffe currents– and derived the corresponding LCSRs for the full set of $\Lambda_b \rightarrow \Lambda$ form factors. While all three interpolating currents lead to formally consistent sum rules, their numerical behaviour differs significantly. In particular, we find that only the pseudoscalar interpolating current yields form factors that exhibit stable Borel behaviour and lead to phenomenologically viable predictions. This observation is consistent with expectations based on the equations of motion and supports the notion that the pseudoscalar current provides the most reliable overlap with the Λ_b ground state in the present framework.

As an important cross-check of our formalism and numerical implementation, we have applied the same sum-rule machinery to the proton case by replacing the Λ -baryon DAs with the

corresponding proton DAs. In doing so, we successfully reproduce the known results of [43], providing a nontrivial validation of our approach. Based on this consistency check and the comparative analysis of interpolating currents, we restrict our subsequent phenomenological discussion to the form factors obtained from the pseudoscalar Λ_b current.

The LCSR s yield the vector and axial-vector form factors $f_i(q^2)$ and $g_i(q^2)$ in the region of low momentum transfer, where the light-cone expansion is expected to converge. To facilitate phenomenological applications and enable comparisons with other nonperturbative approaches, we have transformed these form factors into the helicity basis and parametrised their q^2 dependence using a truncated z -expansion with a single pole factor. This parametrisation provides a smooth interpolation of the LCSR results within their region of validity and allows for a controlled extrapolation in q^2 . Comparisons with lattice-QCD determinations are also presented, where we observe qualitative agreement within uncertainties in the overlapping kinematic region.

Using the form factors obtained in this work, we have computed the differential branching fraction for the rare decay $\Lambda_b \rightarrow \Lambda \ell^+ \ell^-$ in the low- q^2 region. A comparison with the available LHCb data shows that the experimental central values lie systematically below the LCSR-based prediction within the low- q^2 bins. While the present uncertainties prevent a definitive conclusion, this comparison highlights the sensitivity of the decay to hadronic inputs and underlines the need for improved theoretical precision and experimental measurements.

In conclusion, we have demonstrated that LCSR s based on Λ -baryon DAs provide a consistent framework for computing $\Lambda_b \rightarrow \Lambda$ form factors at low momentum transfer. A key outcome of our analysis is the identification of the pseudoscalar Λ_b interpolating current as yielding numerically stable sum rules that satisfy the expected EOM relations and constraints from HQET, once the nearby Λ_b^* contribution is properly accounted for. The resulting form factors enable a controlled phenomenological application to rare Λ_b decays. Our results can be systematically improved by incorporating radiative corrections, tensor operators, and refined inputs for the Λ DAs, and they provide a solid foundation for future studies of rare Λ_b decays and their sensitivity to physics beyond the Standard Model.

Acknowledgment

D.M. is grateful to Siavash Neshatpour for useful discussions.

This research is funded in part by the National Research Agency (ANR) under project no. ANR-21-CE31-0002-01.

A Invariant amplitudes

In this appendix we collect the explicit expressions for the invariant amplitudes appearing in the hadronic representation of the correlation functions with vector and axial-vector weak transition currents. These amplitudes are obtained by inserting complete sets of intermediate Λ_b and Λ_b^* states into the correlation functions and expressing the resulting matrix elements in terms of the corresponding transition form factors defined in Sec 2. The formulas given below are used to construct the hadronic dispersion relations and to identify the structures entering the light-cone sum rules.

For the vector transition current, the hadronic representation of the correlation function $F_\mu^{(l)}(p, q)$ can be written in terms of six independent Lorentz structures, whose coefficients are expressed through the vector form factors $f_i(q^2)$ and $\hat{f}_i(q^2)$ associated with the Λ_b and Λ_b^* intermediate states, respectively:

$$\begin{aligned}
F_\mu^{(l)}(p, q) = & \frac{\lambda_{\Lambda_b}^{(l)} m_{\Lambda_b}}{m_{\Lambda_b}^2 - (p - q)^2} \left[2f_1(q^2) p_\mu - 2\frac{f_2(q^2)}{m_{\Lambda_b}} p_\mu \not{q} + (m_{\Lambda_b} - m_\Lambda) \left(f_1(q^2) - \frac{m_{\Lambda_b} + m_\Lambda}{m_{\Lambda_b}} f_2(q^2) \right) \gamma_\mu \right. \\
& + \left(f_1(q^2) - \frac{m_{\Lambda_b} + m_\Lambda}{m_{\Lambda_b}} f_2(q^2) \right) \gamma_\mu \not{q} + \left(-2f_1(q^2) + \frac{m_{\Lambda_b} + m_\Lambda}{m_{\Lambda_b}} (f_2(q^2) + f_3(q^2)) \right) q_\mu \\
& + \frac{1}{m_{\Lambda_b}} (f_2(q^2) - f_3(q^2)) q_\mu \not{q} \Big] u_\Lambda(P) + \frac{\lambda_{\Lambda_b^*}^{(l)} m_{\Lambda_b^*}}{m_{\Lambda_b^*}^2 - (p - q)^2} \left[-2\hat{f}_1(q^2) P_\mu + 2\frac{\hat{f}_2(q^2)}{m_{\Lambda_b^*}} P_\mu \not{q} \right. \\
& + (m_{\Lambda_b^*} + m_\Lambda) \left(\hat{f}_1(q^2) + \frac{m_{\Lambda_b^*} - m_\Lambda}{m_{\Lambda_b^*}} \hat{f}_2(q^2) \right) \gamma_\mu - \left(\hat{f}_1(q^2) + \frac{m_{\Lambda_b^*} - m_\Lambda}{m_{\Lambda_b}} \hat{f}_2(q^2) \right) \gamma_\mu \not{q} \\
& + \left(2\hat{f}_1(q^2) + \frac{m_{\Lambda_b^*} - m_\Lambda}{m_{\Lambda_b^*}} (\hat{f}_2(q^2) + \hat{f}_3(q^2)) \right) q_\mu - \frac{1}{m_{\Lambda_b^*}} (\hat{f}_2(q^2) - \hat{f}_3(q^2)) q_\mu \not{q} \Big] u_\Lambda(P) \\
& + \int_{s_0^h}^{\infty} \frac{ds}{s - (p - q)^2} \left(\tilde{\rho}_1^{(l)}(s, q^2) p_\mu + \tilde{\rho}_2^{(l)} p_\mu \not{q} + \tilde{\rho}_3^{(l)} \gamma_\mu + \tilde{\rho}_4^{(l)} \gamma_\mu \not{q} + \tilde{\rho}_5^{(l)} q_\mu + \tilde{\rho}_6^{(l)} q_\mu \not{q} \right) u_\Lambda(P). \tag{31}
\end{aligned}$$

In Eq. (31), the first term corresponds to the ground-state Λ_b pole, while the second term arises from the negative-parity excited state Λ_b^* . The quantities $\lambda_{\Lambda_b}^{(l)}$ and $\lambda_{\Lambda_b^*}^{(l)}$ denote the couplings of the interpolating current $\eta_{\Lambda_b}^{(l)}$ to the corresponding baryon states. The functions $\tilde{\rho}_i^{(l)}(s, q^2)$ represent the spectral densities associated with higher resonances and continuum states in the Λ_b channel.

The invariant amplitudes for the axial-vector transition current are obtained analogously. Writing the correlation function $F_{\mu 5}^{(l)}(p, q)$:

$$\begin{aligned}
F_{\mu 5}^{(l)}(P, q) = & \frac{\lambda_{\Lambda_b}^{(l)} m_{\Lambda_b}}{m_{\Lambda_b}^2 - (p - q)^2} \left[2g_1(q^2) p_\mu - 2\frac{g_2(q^2)}{m_{\Lambda_b}} p_\mu \not{q} + (m_{\Lambda_b} - m_\Lambda) \left(g_1(q^2) - \frac{m_{\Lambda_b} + m_\Lambda}{m_{\Lambda_b}} g_2(q^2) \right) \gamma_\mu \right. \\
& + \left(g_1(q^2) - \frac{m_{\Lambda_b} + m_\Lambda}{m_{\Lambda_b}} g_2(q^2) \right) \gamma_\mu \not{q} + \left(-2g_1(q^2) + \frac{m_{\Lambda_b} + m_\Lambda}{m_{\Lambda_b}} (g_2(q^2) + g_3(q^2)) \right) q_\mu \\
& + \frac{1}{m_{\Lambda_b}} (g_2(q^2) - g_3(q^2)) q_\mu \not{q} \Big] u_\Lambda(P) + \frac{\lambda_{\Lambda_b^*}^{(l)} m_{\Lambda_b^*}}{m_{\Lambda_b^*}^2 - (p - q)^2} \left[-2\hat{g}_1(q^2) p_\mu + 2\frac{\hat{g}_2(q^2)}{m_{\Lambda_b^*}} p_\mu \not{q} \right. \\
& \left. \left. + (m_{\Lambda_b^*} + m_\Lambda) \left(\hat{g}_1(q^2) + \frac{m_{\Lambda_b^*} - m_\Lambda}{m_{\Lambda_b^*}} \hat{g}_2(q^2) \right) \gamma_\mu - \left(\hat{g}_1(q^2) + \frac{m_{\Lambda_b^*} - m_\Lambda}{m_{\Lambda_b}} \hat{g}_2(q^2) \right) \gamma_\mu \not{q} \right) u_\Lambda(P) \right].
\end{aligned}$$

$$\begin{aligned}
& + (m_{\Lambda_b^*} + m_\Lambda) \left(\hat{g}_1(q^2) + \frac{m_{\Lambda_b^*} - m_\Lambda}{m_{\Lambda_b^*}} \hat{g}_2(q^2) \right) \gamma_\mu - \left(\hat{g}_1(q^2) + \frac{m_{\Lambda_b^*} - m_\Lambda}{m_{\Lambda_b}} \hat{g}_2(q^2) \right) \gamma_\mu \not{q} \\
& + \left(2\hat{g}_1(q^2) + \frac{m_{\Lambda_b^*} - m_\Lambda}{m_{\Lambda_b^*}} (\hat{g}_2(q^2) + \hat{g}_3(q^2)) \right) q_\mu - \frac{1}{m_{\Lambda_b^*}} (\hat{g}_2(q^2) - \hat{g}_3(q^2)) q_\mu \not{q} \Big] u_\Lambda(P) \\
& + \int_{s_0^h}^\infty \frac{ds}{s - (p - q)^2} \left(\bar{\rho}_1^{(l)}(s, q^2) p_\mu + \bar{\rho}_2^{(l)} p_\mu \not{q} + \bar{\rho}_3^{(l)} \gamma_\mu + \bar{\rho}_4^{(l)} \gamma_\mu \not{q} + \bar{\rho}_5^{(l)} q_\mu + \bar{\rho}_6^{(l)} q_\mu \not{q} \right) u_\Lambda(P). \tag{32}
\end{aligned}$$

Here, $g_i(q^2)$ and $\hat{g}_i(q^2)$ denote the axial-vector form factors for the Λ_b and Λ_b^* transitions, respectively. The Lorentz decomposition is chosen such that the coefficients of the Dirac structures can be directly matched to the invariant amplitudes introduced in Sec 2. As in the vector case, the last term represents the contribution of higher-mass states and the continuum, encoded in the corresponding spectral densities.

B Light Cone Distribution Amplitudes (LCDAs)

In this appendix we summarise the definitions and conventions for the three-quark LCDAs of the Λ baryon used in the light-cone OPE. The LCDAs are defined through vacuum-to- Λ matrix elements of nonlocal three-quark operators near the light-cone and are decomposed into a complete set of Dirac structures multiplied by invariant functions of the longitudinal momentum fractions. We follow the standard conventions of [3, 53]:

$$\begin{aligned}
4 \langle 0 | \epsilon^{ijk} u_\alpha^i(a_1 z) u_\beta^j(a_2 z) s_\gamma^k(a_3 z) | \Lambda(P) \rangle &= \mathcal{S}_1 m_\Lambda C_{\alpha\beta} (\gamma_5 u_\Lambda)_\gamma + \mathcal{S}_2 m_\Lambda^2 C_{\alpha\beta} (\not{z} \gamma_5 u_\Lambda)_\gamma + \mathcal{P}_1 m_\Lambda (\gamma_5 C)_{\alpha\beta} (u_\Lambda)_\gamma \\
&+ \mathcal{P}_2 m_\Lambda^2 (\gamma_5 C)_{\alpha\beta} (\not{z} u_\Lambda)_\gamma + \mathcal{V}_1 (\not{P} C)_{\alpha\beta} (\gamma_5 u_\Lambda)_\gamma + \mathcal{V}_2 m_\Lambda (\not{P} C)_{\alpha\beta} (\not{z} \gamma_5 u_\Lambda)_\gamma + \mathcal{V}_3 m_\Lambda (\gamma_\mu C)_{\alpha\beta} (\gamma^\mu \gamma_5 u_\Lambda)_\gamma \\
&+ \mathcal{V}_4 m_\Lambda^2 (\not{z} C)_{\alpha\beta} (\gamma_5 u_\Lambda)_\gamma + \mathcal{V}_5 m_\Lambda^2 (\gamma_\mu C)_{\alpha\beta} (i\sigma^{\mu\nu} z_\nu \gamma_5 u_\Lambda)_\gamma + \mathcal{V}_6 m_\Lambda^3 (\not{z} C)_{\alpha\beta} (\not{z} \gamma_5 u_\Lambda)_\gamma \\
&+ \mathcal{A}_1 (\not{P} \gamma_5 C)_{\alpha\beta} (u_\Lambda)_\gamma + \mathcal{A}_2 m_\Lambda (\not{P} \gamma_5 C)_{\alpha\beta} (\not{z} u_\Lambda)_\gamma + \mathcal{A}_3 m_\Lambda (\gamma_\mu \gamma_5 C)_{\alpha\beta} (\gamma^\mu u_\Lambda)_\gamma \\
&+ \mathcal{A}_4 m_\Lambda^2 (\not{z} \gamma_5 C)_{\alpha\beta} (u_\Lambda)_\gamma + \mathcal{A}_5 m_\Lambda^2 (\gamma_\mu \gamma_5 C)_{\alpha\beta} (i\sigma^{\mu\nu} z_\nu u_\Lambda)_\gamma + \mathcal{A}_6 m_\Lambda^3 (\not{z} \gamma_5 C)_{\alpha\beta} (\not{z} u_\Lambda)_\gamma \\
&+ \mathcal{T}_1 (P^\nu i\sigma_{\mu\nu} C)_{\alpha\beta} (\gamma^\mu \gamma_5 u_\Lambda)_\gamma + \mathcal{T}_2 m_\Lambda (z^\mu P^\nu i\sigma_{\mu\nu} C)_{\alpha\beta} (\gamma_5 u_\Lambda)_\gamma + \mathcal{T}_3 m_\Lambda (\sigma_{\mu\nu} C)_{\alpha\beta} (\sigma^{\mu\nu} \gamma_5 u_\Lambda)_\gamma \\
&+ \mathcal{T}_4 m_\Lambda (P^\nu \sigma_{\mu\nu} C)_{\alpha\beta} (\sigma^{\mu\rho} z_\rho \gamma_5 u_\Lambda)_\gamma + \mathcal{T}_5 m_\Lambda^2 (z^\nu i\sigma_{\mu\nu} C)_{\alpha\beta} (\gamma^\mu \gamma_5 u_\Lambda)_\gamma + \mathcal{T}_6 m_\Lambda^2 (z^\mu P^\nu i\sigma_{\mu\nu} C)_{\alpha\beta} (\not{z} \gamma_5 u_\Lambda)_\gamma \\
&+ \mathcal{T}_7 m_\Lambda^2 (\sigma_{\mu\nu} C)_{\alpha\beta} (\sigma^{\mu\nu} \not{z} \gamma_5 u_\Lambda)_\gamma + \mathcal{T}_8 m_\Lambda^3 (z^\nu \sigma_{\mu\nu} C)_{\alpha\beta} (\sigma^{\mu\rho} z_\rho \gamma_5 u_\Lambda)_\gamma. \tag{33}
\end{aligned}$$

Here z^μ is a light-like vector ($z^2 = 0$), C denotes the charge-conjugation matrix, and α, β, γ are Dirac indices. The invariant functions $\mathcal{S}_{1,2}$, $\mathcal{P}_{1,2}$, $\mathcal{V}_{1,\dots,6}$, $\mathcal{A}_{1,\dots,6}$, $\mathcal{T}_{1,\dots,8}$ depend on the longitudinal momentum fractions of the constituent quarks and encode the nonperturbative structure of the Λ baryon.

$$\mathcal{M}(a_1, a_2, a_3, (p \cdot z)) = \int dx_1 dx_2 dx_3 \delta(1 - x_1 - x_2 - x_3) e^{-i(p \cdot z) \sum_i x_i a_i} M(x_i). \tag{34}$$

The variables x_i denote the longitudinal momentum fractions carried by the quarks inside the Λ baryon, satisfying $x_1 + x_2 + x_3 = 1$. In the present work we choose the light-cone configuration

\mathcal{M}	integrand on r.h.s. of (34)	\mathcal{M}	integrand on r.h.s. of (34)
\mathcal{S}_1	S_1	$2(p \cdot z) \mathcal{S}_2$	$S_1 - S_2$
\mathcal{P}_1	P_1	$2(p \cdot z) \mathcal{P}_2$	$P_2 - P_1$
\mathcal{V}_1	V_1	$2(p \cdot z) \mathcal{V}_2$	$V_1 - V_2 - V_3$
$2\mathcal{V}_3$	V_3	$4(p \cdot z) \mathcal{V}_4$	$-2V_1 + V_3 + V_4 + 2V_5$
$4(p \cdot z) \mathcal{V}_5$	$V_4 - V_3$	$4(p \cdot z)^2 \mathcal{V}_6$	$-V_1 + V_2 + V_3 + V_4 + V_5 - V_6$
\mathcal{A}_1	A_1	$2(p \cdot z) \mathcal{A}_2$	$-A_1 + A_2 - A_3$
$2\mathcal{A}_3$	A_3	$4(p \cdot z) \mathcal{A}_4$	$-2A_1 - A_3 - A_4 + 2A_5$
$4(p \cdot z) \mathcal{A}_5$	$A_3 - A_4$	$4(p \cdot z)^2 \mathcal{A}_6$	$A_1 - A_2 + A_3 + A_4 - A_5 + A_6$
\mathcal{T}_1	T_1	$2(p \cdot z) \mathcal{T}_2$	$T_1 + T_2 - 2T_3$
$2\mathcal{T}_3$	T_7	$2(p \cdot z) \mathcal{T}_4$	$T_1 - T_2 - 2T_7$
$2(p \cdot z) \mathcal{T}_5$	$-T_1 + T_5 + 2T_8$	$4(p \cdot z)^2 \mathcal{T}_6$	$2T_2 - 2T_3 - 2T_4 + 2T_5 + 2T_7 + 2T_8$
$4(p \cdot z) \mathcal{T}_7$	$T_7 - T_8$	$4(p \cdot z)^2 \mathcal{T}_8$	$-T_1 + T_2 + T_5 - T_6 + 2T_7 + 2T_8$

Table 4: Invariant functions appearing in the decomposition (33) and their relation to the Λ -baryon DAs through Eq. (34).

$a_1 = a_3 = 0$, $a_2 = 1$, corresponding to the strange quark located at position z . The function \mathcal{M} and the integrand on r.h.s. for all coefficients in (33) are collected in Table 4.

The explicit expressions for the Λ -baryon LCDAs up to twist-6 used in this work are listed below.

Twist-3 DAs:

$$V_1 = 0, \quad A_1 = -120 x_1 x_2 x_3 \phi_3^0, \quad T_1 = 0. \quad (35)$$

Twist-4 DAs:

$$\begin{aligned} S_1 &= 6 x_3 (1 - x_3) (\xi_4^0 + \xi_4^{0'}) , & P_1 &= 6 (1 - x_3) (\xi_4^0 - \xi_4^{0'}) , & V_2 &= 0 , \\ V_3 &= 12 (x_1 - x_2) x_3 \psi_4^0 , & A_2 &= -24 x_1 x_2 \phi_4^0 , & A_3 &= -12 x_3 (1 - x_3) \psi_4^0 , \\ T_2 &= 0 , & T_3 &= 6 x_3 (x_2 - x_1) (-\xi_4^0 + \xi_4^{0'}) , & T_7 &= -6 x_3 (x_1 - x_2) (\xi_4^0 + \xi_4^{0'}) . \end{aligned} \quad (36)$$

Twist-5 DAs:

$$\begin{aligned} S_2 &= \frac{3}{2} (x_1 + x_2) (\xi_5^0 + \xi_5^{0'}) , & P_2 &= \frac{3}{2} (x_1 + x_2) (\xi_5^0 - \xi_5^{0'}) , & V_4 &= 3 (x_2 - x_1) \psi_5^0 , \\ V_5 &= 0 , & A_4 &= -3 (1 - x_3) \psi_5^0 , & A_5 &= -6 x_3 \phi_5^0 , & T_4 &= -\frac{3}{2} (x_1 - x_2) (\xi_5^0 + \xi_5^{0'}) , \\ T_5 &= 0 , & T_8 &= -\frac{3}{2} (x_1 - x_2) (\xi_5^0 - \xi_5^{0'}) . \end{aligned} \quad (37)$$

Twist-6 DAs:

$$V_6 = 0, \quad A_6 = -2 \phi_6^0, \quad T_6 = 0. \quad (38)$$

Further, the shorthand notations for combinations of Λ -baryon DA's:

$$\begin{aligned}
S_{12} &= S_1 - S_2, & P_{21} &= P_2 - P_1, \\
V_{1345} &= -2V_1 + V_3 + V_4 + 2V_5, & V_{43} &= V_4 - V_3, \\
V_{123456} &= -V_1 + V_2 + V_3 + V_4 + V_5 - V_6, & V_{123} &= V_1 - V_2 - V_3 \\
A_{1345} &= -2A_1 - A_3 - A_4 + 2A_5, & A_{34} &= A_3 - A_4 \\
A_{123456} &= A_1 - A_2 + A_3 + A_4 - A_5 + A_6, & A_{123} &= -A_1 + A_2 - A_3 \\
T_{78} &= T_7 - T_8, & T_{123} &= T_1 + T_2 - 2T_3, \\
T_{234578} &= 2T_2 - 2T_3 - 2T_4 + 2T_5 + 2T_7 + 2T_8, & T_{127} &= T_1 - T_2 - 2T_7, \\
T_{125678} &= -T_1 + T_2 + T_5 - T_6 + 2T_7 + 2T_8, & T_{158} &= -T_1 + T_5 + 2T_8. \quad (39)
\end{aligned}$$

These DAs enter the light-cone sum rules through convolution integrals with the perturbatively calculable hard-scattering kernels, as described in Sec. 3.

Additionally, the DAs with tildes which come from the integration by parts in x_2 are defined as:

$$\begin{aligned}
\tilde{M}(x_2) &= \int_0^{1-x_2} dx_1 M(x_1, x_2, 1 - x_1 - x_2), \\
\tilde{\tilde{M}}(x_2) &= \int_1^{x_2} dx_2' \int_0^{1-x_2'} dx_1 M(x_1, x_2', 1 - x_1 - x_2'), \\
\tilde{\tilde{\tilde{M}}}(x_2) &= \int_1^{x_2} dx_2' \int_1^{x_2'} dx_2'' \int_0^{1-x_2''} dx_1 M(x_1, x_2'', 1 - x_1 - x_2''). \quad (40)
\end{aligned}$$

We have used the partial integration in the variable x_2 to eliminate $1/p \cdot z$ factors appearing in the DAs.

C QCD representation of correlation functions

In this appendix we present the explicit QCD representations of the correlation functions entering the light-cone sum rules for the $\Lambda_b \rightarrow \Lambda$ transition form factors. The results are organised in terms of invariant amplitudes corresponding to different weak transition currents and interpolating currents for the Λ_b -baryon. The expressions are obtained from the light-cone OPE after performing the replacement of the virtuality $(p - q)^2$ as described in Sec. 3 and are written in terms of convolution integrals of hard-scattering kernels with Λ -baryon LCDAs.

C.1 Pseudoscalar transition current

We first consider the correlation function involving the pseudoscalar weak transition current $j_5 = m_b \bar{s} i \gamma_5 b$. the corresponding invariant amplitudes $F_j^{(i)}((p - q)^2, q^2)$ are defined in Eq. (18) and are expressed below in terms of coefficient functions $T_{jn}^{(i)}$. The explicit expressions are given separately for the pseudoscalar (\mathcal{P}) and axial-vector (\mathcal{A}) interpolating currents of the Λ_b -baryon.

- The pseudoscalar interpolating current:

$$\begin{aligned}
T_{11}^{(\mathcal{P})} &= \frac{m_\Lambda}{2} \left[(m_b - x m_\Lambda) \Phi_1^{(\mathcal{P})} - m_\Lambda \Phi_2^{(\mathcal{P})} \right], \\
T_{12}^{(\mathcal{P})} &= -\frac{m_\Lambda^2}{2} \left[m_b \left(m_b - x m_\Lambda \right) \Phi_2^{(\mathcal{P})} + 2x m_\Lambda^2 \Phi_3^{(\mathcal{P})} \right], \\
T_{13}^{(\mathcal{P})} &= 2m_\Lambda^3 m_b^2 \left(m_b - x m_\Lambda \right) \Phi_3^{(\mathcal{P})}, \\
T_{21}^{(\mathcal{P})} &= -\frac{m_\Lambda}{2} \Phi_1^{(\mathcal{P})}, \quad T_{22}^{(\mathcal{P})} = \frac{m_\Lambda^2}{2} \left(m_b \Phi_2^{(\mathcal{P})} - 2m_\Lambda \Phi_3^{(\mathcal{P})} \right), \\
T_{23}^{(\mathcal{P})} &= -2m_\Lambda^3 m_b^2 \Phi_3^{(\mathcal{P})}, \tag{41}
\end{aligned}$$

where functions $\Phi_i^{(\mathcal{P})}$ in the above equations are:

$$\begin{aligned}
\Phi_1^{(\mathcal{P})} &= 2\tilde{A}_1 + 4\tilde{A}_3 + 2\tilde{A}_{123} + 2\tilde{P}_1 + 2\tilde{S}_1 + 6\tilde{T}_1 - 12\tilde{T}_7 - \tilde{T}_{123} - 5\tilde{T}_{127} \\
&\quad - 2\tilde{V}_1 + 4\tilde{V}_3 + 2\tilde{V}_{123}, \\
\Phi_2^{(\mathcal{P})} &= 3\tilde{\tilde{A}}_{34} + 2\tilde{\tilde{A}}_{123} - \tilde{\tilde{A}}_{1345} - 2\tilde{\tilde{P}}_{21} + 2\tilde{\tilde{S}}_{12} - 12\tilde{\tilde{T}}_{78} - 2\tilde{\tilde{T}}_{123} - 4\tilde{\tilde{T}}_{127} \\
&\quad - 6\tilde{\tilde{T}}_{158} + \tilde{\tilde{T}}_{234578} - 3\tilde{\tilde{V}}_{43} + 2\tilde{\tilde{V}}_{123} + \tilde{\tilde{V}}_{1345}, \\
\Phi_3^{(\mathcal{P})} &= \tilde{\tilde{\tilde{A}}}_{123456} - 3\tilde{\tilde{\tilde{T}}}_{125678} + \tilde{\tilde{\tilde{T}}}_{234578} + \tilde{\tilde{\tilde{V}}}_{123456}.
\end{aligned}$$

Here the shorthand notations \tilde{M} , $\tilde{\tilde{M}}$, and $\tilde{\tilde{\tilde{M}}}$ (where, $M \in \{S, A, V, T, S\}$) denote convolution integrals of the corresponding Λ -baryon DAs defined in Appendix B, with one, two, or three inverse powers of the virtuality Δ , respectively, following the conventions introduced in Sec. 2.

- The axial-vector interpolating current:

$$\begin{aligned}
T_{11}^{(\mathcal{A})} &= 2\frac{m_b^2 - q^2}{x} \Phi_1^{(\mathcal{A})} + x m_\Lambda^2 \left[2\Phi_1^{(\mathcal{A})} + \Phi_2^{(\mathcal{A})} \right] + m_\Lambda m_b \Phi_3^{(\mathcal{A})} + m_\Lambda^2 \left[\Phi_4^{(\mathcal{A})} + \frac{2\Phi_5^{(\mathcal{A})}}{x} \right], \\
T_{12}^{(\mathcal{A})} &= -m_\Lambda^2 \left[2(x^2 m_\Lambda^2 - q^2) \Phi_6^{(\mathcal{A})} + x m_\Lambda m_b \Phi_7^{(\mathcal{A})} + m_b^2 \Phi_8^{(\mathcal{A})} - 2\frac{q^2 + m_b^2}{x} \Phi_5^{(\mathcal{A})} \right. \\
&\quad \left. + 2x m_\Lambda^2 \Phi_9^{(\mathcal{A})} \right], \\
T_{13}^{(\mathcal{A})} &= 4\frac{m_\Lambda^2}{x} \left[m_b^2 (q^2 - m_b^2) \Phi_5^{(\mathcal{A})} - x^2 m_\Lambda^2 m_b^2 \Phi_9^{(\mathcal{A})} + x m_\Lambda m_b^3 \Phi_{10}^{(\mathcal{A})} \right], \\
T_{21}^{(\mathcal{A})} &= \frac{m_\Lambda}{x} \left[2\Phi_6^{(\mathcal{A})} + x \Phi_2^{(\mathcal{A})} \right], \quad T_{23}^{(\mathcal{A})} = 4m_\Lambda^3 m_b^2 \Phi_{11}^{(\mathcal{A})}, \\
T_{22}^{(\mathcal{A})} &= \frac{m_\Lambda}{x} \left[2(q^2 - m_b^2 - x^2 m_\Lambda^2) \Phi_6^{(\mathcal{A})} - x m_\Lambda m_b \Phi_7^{(\mathcal{A})} + 2x m_\Lambda^2 \Phi_{11}^{(\mathcal{A})} \right], \tag{42}
\end{aligned}$$

where the functions $\Phi_i^{(\mathcal{A})}$ are:

$$\begin{aligned}
\Phi_1^{(\mathcal{A})} &= \tilde{A}_1 + 2\tilde{T}_1 + \tilde{V}_1, \\
\Phi_2^{(\mathcal{A})} &= 2\tilde{A}_3 - 2\tilde{P}_1 + 2\tilde{S}_1 - 2\tilde{T}_1 + \tilde{T}_{123} + \tilde{T}_{127} - 2\tilde{V}_3, \\
\Phi_3^{(\mathcal{A})} &= 2\tilde{A}_1 + 4\tilde{A}_3 + 2\tilde{A}_{123} - 4\tilde{P}_1 + 4\tilde{S}_1 + 2\tilde{V}_1 - 4\tilde{V}_3 - 2\tilde{V}_{123}, \\
\Phi_4^{(\mathcal{A})} &= -2\tilde{\tilde{A}}_{1345} + 2\tilde{\tilde{P}}_{21} + 2\tilde{\tilde{S}}_{12} - 2\tilde{\tilde{T}}_{123} + 4\tilde{\tilde{T}}_{127} - 6\tilde{\tilde{T}}_{158} + 3\tilde{\tilde{T}}_{234578} - 2\tilde{\tilde{V}}_{1345}, \\
\Phi_5^{(\mathcal{A})} &= -\tilde{\tilde{T}}_{234578}, \\
\Phi_6^{(\mathcal{A})} &= \tilde{\tilde{A}}_{123} - \tilde{\tilde{T}}_{123} - \tilde{\tilde{T}}_{127} - \tilde{\tilde{V}}_{123}, \\
\Phi_7^{(\mathcal{A})} &= -3\tilde{\tilde{A}}_{34} - 2\tilde{\tilde{A}}_{123} + \tilde{\tilde{A}}_{1345} - 4\tilde{\tilde{P}}_{21} - 4\tilde{\tilde{S}}_{12} - 3\tilde{\tilde{V}}_{43} + 2\tilde{\tilde{V}}_{123} + \tilde{\tilde{V}}_{1345}, \\
\Phi_8^{(\mathcal{A})} &= 2\tilde{\tilde{A}}_{123} + 2\tilde{\tilde{A}}_{1345} - 2\tilde{\tilde{P}}_{21} - 2\tilde{\tilde{S}}_{12} - 6\tilde{\tilde{T}}_{127} + 6\tilde{\tilde{T}}_{158} - 3\tilde{\tilde{T}}_{234578} - 2\tilde{\tilde{V}}_{123} + 2\tilde{\tilde{V}}_{1345}, \\
\Phi_9^{(\mathcal{A})} &= -2\tilde{\tilde{A}}_{123456} + 3\tilde{\tilde{T}}_{125678} - 2\tilde{\tilde{T}}_{234578} + 2\tilde{\tilde{V}}_{123456}, \\
\Phi_{10}^{(\mathcal{A})} &= \tilde{\tilde{\tilde{A}}}_{123456} - \tilde{\tilde{\tilde{V}}}_{123456}, \\
\Phi_{11}^{(\mathcal{A})} &= 2\tilde{\tilde{\tilde{A}}}_{123456} - 3\tilde{\tilde{\tilde{T}}}_{125678} + \tilde{\tilde{\tilde{T}}}_{234578} - 2\tilde{\tilde{\tilde{V}}}_{123456}.
\end{aligned}$$

C.2 Vector transition current

We next present the invariant amplitudes for the correlation function involving the vector weak transition current $j_\mu = \bar{s}\gamma_\mu b$. The invariant amplitudes $\tilde{F}_j^{(i)}((p-q)^2, q^2)$ for the correlation function with the vector transition current j_μ are given by Eq. (18) with the replacement of the coefficient $m_b/4 \rightarrow 1/4$. The coefficient functions $\tilde{T}_{jn}^{(i)}$ with $i = \mathcal{P}, \mathcal{A}$, $j = 1, 2, \dots 6$ and $n = 1, 2, 3$ are listed below for:

- The pseudoscalar interpolating current:

$$\begin{aligned}
\tilde{T}_{11}^{(\mathcal{P})} &= x m_\Lambda \tilde{\Phi}_1^{(\mathcal{P})}, & \tilde{T}_{12}^{(\mathcal{P})} &= x m_\Lambda^3 \left[x \tilde{\Phi}_2^{(\mathcal{P})} + 2\tilde{\Phi}_3^{(\mathcal{P})} \right], \\
\tilde{T}_{13}^{(\mathcal{P})} &= 4x m_\Lambda^3 m_b^2 \tilde{\Phi}_3^{(\mathcal{P})}, \\
\tilde{T}_{21}^{(\mathcal{P})} &= \tilde{T}_{23}^{(\mathcal{P})} = 0, & \tilde{T}_{22}^{(\mathcal{P})} &= -x m_\Lambda^2 \tilde{\Phi}_2^{(\mathcal{P})}, \\
\tilde{T}_{31}^{(\mathcal{P})} &= \frac{m_\Lambda}{2} (m_b - x m_\Lambda) \tilde{\Phi}_1^{(\mathcal{P})}, \\
\tilde{T}_{32}^{(\mathcal{P})} &= -\frac{m_\Lambda^2}{2} \left[m_b (m_b - x m_\Lambda) \tilde{\Phi}_2^{(\mathcal{P})} + 2x m_\Lambda^2 \tilde{\Phi}_3^{(\mathcal{P})} \right], \\
\tilde{T}_{33}^{(\mathcal{P})} &= 2m_\Lambda^3 m_b^2 (m_b - x m_\Lambda) \tilde{\Phi}_3^{(\mathcal{P})}, \\
\tilde{T}_{41}^{(\mathcal{P})} &= \frac{m_\Lambda}{2} \tilde{\Phi}_1^{(\mathcal{P})}, & \tilde{T}_{42}^{(\mathcal{P})} &= \frac{m_\Lambda^2}{2} \left[-m_b \tilde{\Phi}_2^{(\mathcal{P})} + 2m_\Lambda \tilde{\Phi}_3^{(\mathcal{P})} \right], \\
\tilde{T}_{43}^{(\mathcal{P})} &= 2m_\Lambda^3 m_b^2 \tilde{\Phi}_3^{(\mathcal{P})},
\end{aligned}$$

$$\begin{aligned}
\tilde{T}_{51}^{(\mathcal{P})} &= -m_\Lambda \tilde{\Phi}_1^{(\mathcal{P})}, & \tilde{T}_{52}^{(\mathcal{P})} &= -m_\Lambda^3 \left[x \tilde{\Phi}_2^{(\mathcal{P})} + 2 \tilde{\Phi}_3^{(\mathcal{P})} \right], \\
\tilde{T}_{53}^{(\mathcal{P})} &= -4m_\Lambda^3 m_b^2 \tilde{\Phi}_3^{(\mathcal{P})}, \\
\tilde{T}_{61}^{(\mathcal{P})} &= \tilde{T}_{63}^{(\mathcal{P})} = 0, & \tilde{T}_{62}^{(\mathcal{P})} &= m_\Lambda^2 \tilde{\Phi}_2^{(\mathcal{P})}, \tag{43}
\end{aligned}$$

where the functions $\tilde{\Phi}_i^{(\mathcal{P})}$ are given by:

$$\begin{aligned}
\tilde{\Phi}_1^{(\mathcal{P})} &= 2\tilde{A}_1 + 4\tilde{A}_3 + 2\tilde{A}_{123} + 2\tilde{P}_1 + 2\tilde{S}_1 + 6\tilde{T}_1 - 12\tilde{T}_7 - \tilde{T}_{123} - 5\tilde{T}_{127} \\
&\quad - 2\tilde{V}_1 + 4\tilde{V}_3 + 2\tilde{V}_{123}, \\
\tilde{\Phi}_2^{(\mathcal{P})} &= 3\tilde{A}_{34} + 2\tilde{A}_{123} - \tilde{A}_{1345} - 2\tilde{P}_{21} + 2\tilde{S}_{12} - 12\tilde{T}_{78} - 2\tilde{T}_{123} - 4\tilde{T}_{127} \\
&\quad - 6\tilde{T}_{158} + \tilde{T}_{234578} - 3\tilde{V}_{43} + 2\tilde{V}_{123} + \tilde{V}_{1345}, \\
\tilde{\Phi}_3^{(\mathcal{P})} &= \tilde{A}_{123456} - 3\tilde{T}_{125678} + \tilde{T}_{234578} + \tilde{V}_{123456}.
\end{aligned}$$

- The axial-vector interpolating current:

$$\begin{aligned}
\tilde{T}_{11}^{(\mathcal{A})} &= 2 \left[2m_b \tilde{\Phi}_1^{(\mathcal{A})} - x m_\Lambda (2\tilde{\Phi}_1^{(\mathcal{A})} + \tilde{\Phi}_2^{(\mathcal{A})}) + 2m_\Lambda \tilde{\Phi}_3^{(\mathcal{A})} \right], \\
\tilde{T}_{12}^{(\mathcal{A})} &= 2m_\Lambda \left[x^2 m_\Lambda^2 \tilde{\Phi}_4^{(\mathcal{A})} + x m_\Lambda m_b \tilde{\Phi}_5^{(\mathcal{A})} + 2m_b^2 \tilde{\Phi}_3^{(\mathcal{A})} + 2x m_\Lambda^2 \tilde{\Phi}_6^{(\mathcal{A})} \right], \\
\tilde{T}_{13}^{(\mathcal{A})} &= 8m_\Lambda^2 m_b \left[m_b^2 \tilde{\Phi}_7^{(\mathcal{A})} + x m_\Lambda m_b \tilde{\Phi}_6^{(\mathcal{A})} + x^2 m_\Lambda^2 \tilde{\Phi}_8^{(\mathcal{A})} \right], \\
\tilde{T}_{21}^{(\mathcal{A})} &= 4\tilde{\Phi}_1^{(\mathcal{A})}, & \tilde{T}_{23}^{(\mathcal{A})} &= 8m_\Lambda^2 m_b \left[m_b \tilde{\Phi}_7^{(\mathcal{A})} - x m_\Lambda \tilde{\Phi}_8^{(\mathcal{A})} \right], \\
\tilde{T}_{22}^{(\mathcal{A})} &= 2m_\Lambda \left[2m_b \tilde{\Phi}_3^{(\mathcal{A})} - x m_\Lambda \tilde{\Phi}_4^{(\mathcal{A})} + 2m_\Lambda \tilde{\Phi}_7^{(\mathcal{A})} \right], \\
\tilde{T}_{31}^{(\mathcal{A})} &= 2 \frac{m_b^2 - q^2}{x} \tilde{\Phi}_1^{(\mathcal{A})} + m_\Lambda m_b \tilde{\Phi}_2^{(\mathcal{A})} + m_\Lambda^2 \tilde{\Phi}_9^{(\mathcal{A})} - 2x m_\Lambda^2 \tilde{\Phi}_{10}^{(\mathcal{A})} - 2 \frac{m_\Lambda^2}{x} \tilde{\Phi}_7^{(\mathcal{A})}, \\
\tilde{T}_{32}^{(\mathcal{A})} &= m_\Lambda^2 \left[2(q^2 - x^2 m_\Lambda^2) \tilde{\Phi}_3^{(\mathcal{A})} - 2 \frac{q^2 + m_b^2}{x} \tilde{\Phi}_7^{(\mathcal{A})} + x m_\Lambda m_b \tilde{\Phi}_{11}^{(\mathcal{A})} \right. \\
&\quad \left. + m_b^2 (\tilde{\Phi}_5^{(\mathcal{A})} - 2\tilde{\Phi}_3^{(\mathcal{A})}) + 2m_\Lambda (m_b + x m_\Lambda) \tilde{\Phi}_8^{(\mathcal{A})} \right], \\
\tilde{T}_{33}^{(\mathcal{A})} &= \frac{4m_b^2 m_\Lambda^2}{x} \left[(m_b^2 - q^2) \tilde{\Phi}_7^{(\mathcal{A})} + x m_\Lambda m_b \tilde{\Phi}_{12}^{(\mathcal{A})} + x^2 m_\Lambda^2 \tilde{\Phi}_8^{(\mathcal{A})} \right], \\
\tilde{T}_{41}^{(\mathcal{A})} &= 2m_\Lambda \left[(\tilde{\Phi}_1^{(\mathcal{A})} + \tilde{\Phi}_{10}^{(\mathcal{A})}) - \frac{\tilde{\Phi}_3^{(\mathcal{A})}}{x} \right], & \tilde{T}_{43}^{(\mathcal{A})} &= 4m_\Lambda^3 m_b^2 \tilde{\Phi}_{13}^{(\mathcal{A})}, \\
\tilde{T}_{42}^{(\mathcal{A})} &= \frac{m_\Lambda}{x} \left[2(m_b^2 + x^2 m_\Lambda^2 - q^2) \tilde{\Phi}_3^{(\mathcal{A})} - x m_\Lambda m_b \tilde{\Phi}_{11}^{(\mathcal{A})} + 2x m_\Lambda^2 \tilde{\Phi}_{13}^{(\mathcal{A})} \right],
\end{aligned}$$

$$\begin{aligned}
\tilde{T}_{51}^{(\mathcal{A})} &= 2m_\Lambda \tilde{\Phi}_2^{(\mathcal{A})}, & \tilde{T}_{53}^{(\mathcal{A})} &= 8m_\Lambda^3 m_b \left[m_b \tilde{\Phi}_{14}^{(\mathcal{A})} - x m_\Lambda \tilde{\Phi}_8^{(\mathcal{A})} \right], \\
\tilde{T}_{52}^{(\mathcal{A})} &= 2m_\Lambda^2 \left[-x m_\Lambda \tilde{\Phi}_4^{(\mathcal{A})} - m_b (\tilde{\Phi}_5^{(\mathcal{A})} + 2\tilde{\Phi}_3^{(\mathcal{A})}) + 2m_\Lambda \tilde{\Phi}_{14}^{(\mathcal{A})} \right], \\
\tilde{T}_{61}^{(\mathcal{A})} &= 0, & \tilde{T}_{62}^{(\mathcal{A})} &= 2m_\Lambda^2 \tilde{\Phi}_4^{(\mathcal{A})}, & \tilde{T}_{63}^{(\mathcal{A})} &= 8m_\Lambda^3 m_b \tilde{\Phi}_8^{(\mathcal{A})}. \tag{44}
\end{aligned}$$

The functions $\tilde{\Phi}_i^{(\mathcal{A})}$ are given by:

$$\begin{aligned}
\tilde{\Phi}_1^{(\mathcal{A})} &= \tilde{A}_1 + 2\tilde{T}_1 + \tilde{V}_1, \\
\tilde{\Phi}_2^{(\mathcal{A})} &= 2\tilde{A}_3 - 2\tilde{P}_1 + 2\tilde{S}_1 - 2\tilde{T}_1 + \tilde{T}_{123} + \tilde{T}_{127} - 2\tilde{V}_3, \\
\tilde{\Phi}_3^{(\mathcal{A})} &= \tilde{\tilde{A}}_{123} - \tilde{\tilde{T}}_{123} - \tilde{\tilde{T}}_{127} - \tilde{\tilde{V}}_{123}, \\
\tilde{\Phi}_4^{(\mathcal{A})} &= -\tilde{\tilde{A}}_{34} + \tilde{\tilde{A}}_{1345} - 2\tilde{\tilde{P}}_{21} - 2\tilde{\tilde{S}}_{12} - 2\tilde{\tilde{T}}_{127} + 2\tilde{\tilde{T}}_{158} - \tilde{\tilde{T}}_{234578} - \tilde{\tilde{V}}_{43} + \tilde{\tilde{V}}_{1345}, \\
\tilde{\Phi}_5^{(\mathcal{A})} &= -\tilde{\tilde{A}}_{34} - 2\tilde{\tilde{A}}_{123} - \tilde{\tilde{A}}_{1345} + 4\tilde{\tilde{T}}_{127} - 4\tilde{\tilde{T}}_{158} + 2\tilde{\tilde{T}}_{234578} - \tilde{\tilde{V}}_{43} + 2\tilde{\tilde{V}}_{123} - \tilde{\tilde{V}}_{1345}, \\
\tilde{\Phi}_6^{(\mathcal{A})} &= -\tilde{\tilde{\tilde{A}}}_{123456} + \tilde{\tilde{\tilde{T}}}_{125678} - \tilde{\tilde{\tilde{T}}}_{234578} + \tilde{\tilde{\tilde{V}}}_{123456}, \\
\tilde{\Phi}_7^{(\mathcal{A})} &= \tilde{\tilde{\tilde{T}}}_{234578}, \\
\tilde{\Phi}_8^{(\mathcal{A})} &= \tilde{\tilde{\tilde{A}}}_{123456} - 2\tilde{\tilde{\tilde{T}}}_{125678} + \tilde{\tilde{\tilde{T}}}_{234578} - \tilde{\tilde{\tilde{V}}}_{123456}, \\
\tilde{\Phi}_9^{(\mathcal{A})} &= -2\tilde{\tilde{A}}_{34} - 2\tilde{\tilde{A}}_{123} - 2\tilde{\tilde{P}}_{21} - 2\tilde{\tilde{S}}_{12} + 2\tilde{\tilde{T}}_{127} - 2\tilde{\tilde{T}}_{158} + \tilde{\tilde{T}}_{234578} - 2\tilde{\tilde{V}}_{43} + 2\tilde{\tilde{V}}_{123}, \\
\tilde{\Phi}_{10}^{(\mathcal{A})} &= \tilde{\tilde{A}}_{123} - \tilde{\tilde{T}}_{123} - \tilde{\tilde{T}}_{127} - \tilde{\tilde{V}}_{123}, \\
\tilde{\Phi}_{11}^{(\mathcal{A})} &= 2\tilde{\tilde{A}}_{34} + 2\tilde{\tilde{P}}_{21} + 2\tilde{\tilde{S}}_{12} + 2\tilde{\tilde{T}}_{123} + 2\tilde{\tilde{T}}_{158} - \tilde{\tilde{T}}_{234578} + 2\tilde{\tilde{V}}_{43}, \\
\tilde{\Phi}_{12}^{(\mathcal{A})} &= \tilde{\tilde{\tilde{T}}}_{125678} - \tilde{\tilde{\tilde{T}}}_{234578}, \\
\tilde{\Phi}_{13}^{(\mathcal{A})} &= -\tilde{\tilde{\tilde{A}}}_{123456} + 2\tilde{\tilde{\tilde{T}}}_{125678} + \tilde{\tilde{\tilde{V}}}_{123456}, \\
\tilde{\Phi}_{14}^{(\mathcal{A})} &= \tilde{\tilde{T}}_1^M + \tilde{\tilde{\tilde{A}}}_{123456} - \tilde{\tilde{\tilde{T}}}_{125678} - \tilde{\tilde{\tilde{V}}}_{123456}.
\end{aligned}$$

C.3 axial-vector transition current

The invariant amplitude for the axial-vector weak transition current $j_{\mu 5} = \bar{s} \gamma_\mu \gamma_5 b$ are obtained analogously. The invariant amplitudes $\bar{F}_j^{(i)}((p-q)^2, q^2)$ corresponding to the axial-vector transition current are obtained from the vector-current expressions by reversing the sign of the heavy-quark mass m_b , reflecting the opposite parity of the axial current. In addition, sign changes occur for the specific coefficient functions $\tilde{T}_{2n}^{(\mathcal{P})}$, $\tilde{T}_{3n}^{(\mathcal{P})}$, $\tilde{T}_{6n}^{(\mathcal{P})}$, $\tilde{T}_{1n}^{(\mathcal{A})}$, $\tilde{T}_{4n}^{(\mathcal{A})}$ and $\tilde{T}_{5n}^{(\mathcal{A})}$, as dictated by the Dirac structure of the corresponding invariant amplitudes.

D Differential decay-width of $\Lambda_b \rightarrow \Lambda \ell^+ \ell^-$

We consider the effective Hamiltonian restricted to semileptonic operators with vector, axial-vector, and tensor quark currents,

$$\begin{aligned} \mathcal{H}_{\text{eff}} \supset & -\frac{4G_F}{\sqrt{2}} V_{tb}^* V_{ts} \frac{\alpha_{em}}{4\pi} [C_9^{\text{eff}} (\bar{s} \gamma_\mu P_L b) (\bar{\ell} \gamma^\mu \ell) + C_{10} (\bar{s} \gamma_\mu P_L b) (\bar{\ell} \gamma^\mu \gamma_5 \ell) \\ & + \frac{2m_b}{q^2} C_7^{\text{eff}} (\bar{s} i \sigma_{\mu\nu} q^\nu P_R b) (\bar{\ell} \gamma^\mu \ell)], \end{aligned} \quad (45)$$

where $P_{L,R} = (1 \mp \gamma_5)/2$. The hadronic matrix elements of the vector and axial-vector currents are expressed in terms of the helicity form factors $F \in \{f_+, f_\perp, g_+, g_\perp\}$ determined in this work using LCSR and subsequently extrapolated in q^2 . The tensor form factors $h_+(q^2)$, $h_\perp(q^2)$ and their axial counterparts $\tilde{h}_+(q^2)$, $\tilde{h}_\perp(q^2)$ are not computed within the present LCSR framework and are instead taken from lattice-QCD determinations.

The following shorthand is used in the differential decay width,

$$\begin{aligned} \mathcal{N} = & \frac{G_F^2 \alpha_{em}^2 |V_{ts}^* V_{tb}|^2}{3 \cdot 2^8 \pi^5 m_{\Lambda_b}^3}, \quad s_\pm = (m_{\Lambda_b} \pm m_\Lambda)^2 - q^2, \\ \lambda \equiv & \lambda(m_{\Lambda_b}^2, m_\Lambda^2, q^2) = s_+ s_-. \end{aligned} \quad (46)$$

In the massless-lepton limit, the differential decay width can be written as:

$$\frac{d\Gamma(\Lambda_b \rightarrow \Lambda \ell^+ \ell^-)}{dq^2} = \mathcal{N} \sqrt{\lambda} q^2 [2H_T(q^2) + H_L(q^2)], \quad (47)$$

and the transverse and longitudinal contributions given by:

$$\begin{aligned} H_T(q^2) = & \left[s_- \left(\left| C_9^{\text{eff}}(q^2) f_\perp(q^2) + \frac{2m_b(m_{\Lambda_b} + m_\Lambda) C_7^{\text{eff}}}{q^2} h_\perp(q^2) \right|^2 + |C_{10} f_\perp(q^2)|^2 \right) \right. \\ & \left. + s_+ \left(\left| C_9^{\text{eff}}(q^2) g_\perp(q^2) + \frac{2m_b(m_{\Lambda_b} - m_\Lambda) C_7^{\text{eff}}}{q^2} \tilde{h}_\perp(q^2) \right|^2 + |C_{10} g_\perp(q^2)|^2 \right) \right], \\ H_L(q^2) = & \frac{1}{q^2} \left[s_- (m_{\Lambda_b} + m_\Lambda)^2 \left(\left| C_9^{\text{eff}}(q^2) f_+(q^2) + \frac{2m_b C_7^{\text{eff}}}{(m_{\Lambda_b} + m_\Lambda)} h_+(q^2) \right|^2 + |C_{10} f_+(q^2)|^2 \right) \right. \\ & \left. + s_+ (m_{\Lambda_b} - m_\Lambda)^2 \left(\left| C_9^{\text{eff}}(q^2) g_+(q^2) + \frac{2m_b C_7^{\text{eff}}}{(m_{\Lambda_b} - m_\Lambda)} \tilde{h}_+(q^2) \right|^2 + |C_{10} g_+(q^2)|^2 \right) \right]. \end{aligned} \quad (48)$$

References

- [1] T. Hurth, F. Mahmoudi, Y. Monceaux, and S. Neshatpour, *Data-driven analyses and model-independent fits for present $b \rightarrow s \ell \ell$ results*, *Phys. Rev. D* **112** (2025), no. 11 113003, [[arXiv:2508.09986](https://arxiv.org/abs/2508.09986)].
- [2] C.-H. Chen and C. Q. Geng, *Baryonic rare decays of $\Lambda_b \rightarrow \Lambda \ell^+ \ell^-$* , *Phys. Rev. D* **64** (2001) 074001, [[hep-ph/0106193](https://arxiv.org/abs/hep-ph/0106193)].

- [3] T. M. Aliev, K. Azizi, and M. Savci, *Analysis of the $\Lambda_b \rightarrow \Lambda \ell^+ \ell^-$ decay in QCD*, *Phys. Rev. D* **81** (2010) 056006, [[arXiv:1001.0227](https://arxiv.org/abs/1001.0227)].
- [4] **CDF** Collaboration, T. Aaltonen et al., *Observation of the Baryonic Flavor-Changing Neutral Current Decay $\Lambda_b \rightarrow \Lambda \mu^+ \mu^-$* , *Phys. Rev. Lett.* **107** (2011) 201802, [[arXiv:1107.3753](https://arxiv.org/abs/1107.3753)].
- [5] W. Detmold, C. J. D. Lin, S. Meinel, and M. Wingate, *$\Lambda_b \rightarrow \Lambda \ell^+ \ell^-$ form factors and differential branching fraction from lattice QCD*, *Phys. Rev. D* **87** (2013), no. 7 074502, [[arXiv:1212.4827](https://arxiv.org/abs/1212.4827)].
- [6] **LHCb** Collaboration, R. Aaij et al., *Measurement of the differential branching fraction of the decay $\Lambda_b^0 \rightarrow \Lambda \mu^+ \mu^-$* , *Phys. Lett. B* **725** (2013) 25–35, [[arXiv:1306.2577](https://arxiv.org/abs/1306.2577)].
- [7] Y. Liu, L. L. Liu, and X. H. Guo, *Study of $\Lambda_b \rightarrow \Lambda l^+ l^-$ and $\Lambda_b \rightarrow p l \bar{\nu}$ decays in the Bethe-Salpeter equation approach*, [arXiv:1503.06907](https://arxiv.org/abs/1503.06907).
- [8] **LHCb** Collaboration, R. Aaij et al., *Differential branching fraction and angular analysis of $\Lambda_b^0 \rightarrow \Lambda \mu^+ \mu^-$ decays*, *JHEP* **06** (2015) 115, [[arXiv:1503.07138](https://arxiv.org/abs/1503.07138)]. [Erratum: *JHEP* 09, 145 (2018)].
- [9] S. Meinel and D. van Dyk, *Using $\Lambda_b \rightarrow \Lambda \mu^+ \mu^-$ data within a Bayesian analysis of $|\Delta B| = |\Delta S| = 1$ decays*, *Phys. Rev. D* **94** (2016), no. 1 013007, [[arXiv:1603.02974](https://arxiv.org/abs/1603.02974)].
- [10] R. N. Faustov and V. O. Galkin, *Rare $\Lambda_b \rightarrow \Lambda l^+ l^-$ and $\Lambda_b \rightarrow \Lambda \gamma$ decays in the relativistic quark model*, *Phys. Rev. D* **96** (2017), no. 5 053006, [[arXiv:1705.07741](https://arxiv.org/abs/1705.07741)].
- [11] S. Bhattacharya, S. Nandi, S. K. Patra, and R. Sain, *Detailed study of the $\Lambda_b \rightarrow \Lambda \ell^+ \ell^-$ decays in the standard model*, *Phys. Rev. D* **101** (2020), no. 7 073006, [[arXiv:1912.06148](https://arxiv.org/abs/1912.06148)].
- [12] S. Meinel and G. Rendon, *$\Lambda_b \rightarrow \Lambda^*(1520) \ell^+ \ell^-$ form factors from lattice QCD*, *Phys. Rev. D* **103** (2021), no. 7 074505, [[arXiv:2009.09313](https://arxiv.org/abs/2009.09313)].
- [13] M. Bordone, *Heavy Quark Expansion of $\Lambda_b \rightarrow \Lambda^*(1520)$ Form Factors beyond Leading Order*, *Symmetry* **13** (2021), no. 4 531, [[arXiv:2101.12028](https://arxiv.org/abs/2101.12028)].
- [14] T. Blake, S. Meinel, M. Rahimi, and D. van Dyk, *Dispersive bounds for local form factors in $\Lambda_b \rightarrow \Lambda$ transitions*, *Phys. Rev. D* **108** (2023), no. 9 094509, [[arXiv:2205.06041](https://arxiv.org/abs/2205.06041)].
- [15] Y. Amhis, M. Bordone, and M. Reboud, *Dispersive analysis of $\Lambda_b \rightarrow \Lambda(1520)$ local form factors*, *JHEP* **02** (2023) 010, [[arXiv:2208.08937](https://arxiv.org/abs/2208.08937)].
- [16] L.-S. Lu, C.-D. Lü, Y.-L. Shen, and Y.-B. Wei, *SCET sum rules for $\Lambda_b \rightarrow \Lambda \ell^+ \ell^- (\Lambda \gamma)$ decays*, *JHEP* **09** (2025) 172, [[arXiv:2506.21419](https://arxiv.org/abs/2506.21419)].
- [17] D. Das and J. Das, *The $\Lambda_b \rightarrow \Lambda^*(1520) (\rightarrow N \bar{K}) \ell^+ \ell^-$ decay at low-recoil in HQET*, *JHEP* **07** (2020) 002, [[arXiv:2003.08366](https://arxiv.org/abs/2003.08366)].
- [18] T. Gutsche, M. A. Ivanov, J. G. Korner, V. E. Lyubovitskij, and P. Santorelli, *Rare baryon decays $\Lambda_b \rightarrow \Lambda l^+ l^- (l = e, \mu, \tau)$ and $\Lambda_b \rightarrow \Lambda \gamma$: differential and total rates, lepton- and hadron-side forward-backward asymmetries*, *Phys. Rev. D* **87** (2013) 074031, [[arXiv:1301.3737](https://arxiv.org/abs/1301.3737)].

[19] P. Böer, T. Feldmann, and D. van Dyk, *Angular Analysis of the Decay $\Lambda_b \rightarrow \Lambda(\rightarrow N\pi)\ell^+\ell^-$* , *JHEP* **01** (2015) 155, [[arXiv:1410.2115](https://arxiv.org/abs/1410.2115)].

[20] G. Kumar and N. Mahajan, *Asymmetries and observables for $\Lambda_b \rightarrow \Lambda\ell^+\ell^-$* , [arXiv:1511.00935](https://arxiv.org/abs/1511.00935).

[21] T. Blake and M. Kreps, *Angular distribution of polarised Λ_b baryons decaying to $\Lambda\ell^+\ell^-$* , *JHEP* **11** (2017) 138, [[arXiv:1710.00746](https://arxiv.org/abs/1710.00746)].

[22] S. Descotes-Genon and M. Novoa-Brunet, *Angular analysis of the rare decay $\Lambda_b \rightarrow \Lambda(1520)(\rightarrow NK)\ell^+\ell^-$* , *JHEP* **06** (2019) 136, [[arXiv:1903.00448](https://arxiv.org/abs/1903.00448)]. [Erratum: *JHEP* 06, 102 (2020)].

[23] Y.-S. Li, S.-P. Jin, J. Gao, and X. Liu, *Transition form factors and angular distributions of the $\Lambda_b \rightarrow \Lambda(1520)(\rightarrow NK^-)\ell^+\ell^-$ decay supported by baryon spectroscopy*, *Phys. Rev. D* **107** (2023), no. 9 093003, [[arXiv:2210.04640](https://arxiv.org/abs/2210.04640)].

[24] R. Khan, F. M. Bhutta, I. Ahmed, and M. J. Aslam, *Lepton polarization dependent angular observables and the polarization asymmetries in the four-fold $\Lambda_b \rightarrow \Lambda(\rightarrow N\pi)\ell^+\ell^-$ decay*, [arXiv:2510.00249](https://arxiv.org/abs/2510.00249).

[25] G. Hiller and A. Kagan, *Probing for new physics in polarized Λ_b decays at the Z* , *Phys. Rev. D* **65** (2002) 074038, [[hep-ph/0108074](https://arxiv.org/abs/hep-ph/0108074)].

[26] M. J. Aslam, Y.-M. Wang, and C.-D. Lu, *Exclusive semileptonic decays of $\Lambda_b \rightarrow \Lambda l^+l^-$ in supersymmetric theories*, *Phys. Rev. D* **78** (2008) 114032, [[arXiv:0808.2113](https://arxiv.org/abs/0808.2113)].

[27] Y.-M. Wang, M. J. Aslam, and C.-D. Lu, *Rare decays of $\Lambda_b \rightarrow \Lambda\gamma$ and $\Lambda_b \rightarrow \Lambda l^+l^-$ in universal extra dimension model*, *Eur. Phys. J. C* **59** (2009) 847–860, [[arXiv:0810.0609](https://arxiv.org/abs/0810.0609)].

[28] S. Sahoo, C. K. Das, and L. Maharana, *Effect of both Z and Z -prime mediated flavor-changing neutral currents on the baryonic rare decay $\Lambda_b \rightarrow \Lambda l^+l^-$* , *Int. J. Mod. Phys. A* **24** (2009) 6223–6235, [[arXiv:1112.4563](https://arxiv.org/abs/1112.4563)].

[29] K. Azizi, S. Kartal, A. T. Olgun, and Z. Tavukoglu, *Analysis of the semileptonic $\Lambda_b \rightarrow \Lambda\ell^+\ell^-$ transition in the topcolor-assisted technicolor model*, *Phys. Rev. D* **88** (2013), no. 7 075007, [[arXiv:1307.3101](https://arxiv.org/abs/1307.3101)].

[30] K. Azizi, A. T. Olgun, and Z. Tavukoglu, *Comparative analysis of the $\Lambda_b \rightarrow \Lambda\ell^+\ell^-$ decay in the SM, SUSY and RS model with custodial protection*, *Phys. Rev. D* **92** (2015), no. 11 115025, [[arXiv:1508.03980](https://arxiv.org/abs/1508.03980)].

[31] S.-W. Wang and J.-S. Huang, *Two Higgs Doublet Model III and Double-Lepton Polarization Asymmetries in $\Lambda_b \rightarrow \Lambda\mu^+\mu^-$ Decays*, *Commun. Theor. Phys.* **66** (2016), no. 2 211–218.

[32] S.-W. Wang and Y.-D. Yang, *Analysis of $\Lambda_b \rightarrow \Lambda\mu^+\mu^-$ decay in scalar leptoquark model*, *Adv. High Energy Phys.* **2016** (2016) 5796131, [[arXiv:1608.03662](https://arxiv.org/abs/1608.03662)].

[33] R. F. Alnahdi, T. Barakat, and H. A. Alhendi, *Rare $\Lambda_b \rightarrow \Lambda\ell^+\ell^-$ decay in the two-Higgs doublet model of type-III*, *PTEP* **2017** (2017), no. 7 073B04, [[arXiv:1706.07361](https://arxiv.org/abs/1706.07361)].

[34] D. Das, *Model independent New Physics analysis in $\Lambda_b \rightarrow \Lambda \mu^+ \mu^-$ decay*, *Eur. Phys. J. C* **78** (2018), no. 3 230, [[arXiv:1802.09404](https://arxiv.org/abs/1802.09404)].

[35] A. Nasrullah, M. Jamil Aslam, and S. Shafaq, *Analysis of angular observables of $\Lambda_b \rightarrow \Lambda (\rightarrow p\pi) \mu^+ \mu^-$ decay in the standard and Z' models*, *PTEP* **2018** (2018), no. 4 043B08, [[arXiv:1803.06885](https://arxiv.org/abs/1803.06885)].

[36] A. Nasrullah, F. M. Bhutta, and M. J. Aslam, *The $\Lambda_b \rightarrow \Lambda (\rightarrow p\pi^-) \mu^+ \mu^-$ decay in the RS_c model*, *J. Phys. G* **45** (2018), no. 9 095007, [[arXiv:1805.01393](https://arxiv.org/abs/1805.01393)].

[37] A. Nasrullah, I. Ahmed, M. J. Aslam, Z. Asghar, and S. Shafaq, *Probing new physics effects in $\Lambda_b \rightarrow \Lambda (\rightarrow p\pi^-) \ell^+ \ell^-$ decay via model-independent approach*, *Phys. Scripta* **96** (2021), no. 12 125309, [[arXiv:2006.15513](https://arxiv.org/abs/2006.15513)].

[38] Y. Amhis, S. Descotes-Genon, C. Marin Benito, M. Novoa-Brunet, and M.-H. Schune, *Prospects for New Physics searches with $\Lambda_b^0 \rightarrow \Lambda(1520) \ell^+ \ell^-$ decays*, *Eur. Phys. J. Plus* **136** (2021), no. 6 614, [[arXiv:2005.09602](https://arxiv.org/abs/2005.09602)].

[39] D. Das, J. Das, G. Kumar, and N. Sahoo, $\Lambda_b \rightarrow \Lambda (\rightarrow p\pi^-) \ell^+ \ell^-$ as probe of CP -violating new physics, *Phys. Rev. D* **108** (2023), no. 1 015001, [[arXiv:2211.09065](https://arxiv.org/abs/2211.09065)].

[40] S. Biswas, S. Mahata, B. P. Nayak, and S. Sahoo, *Imprints of new physics in $\Lambda_b \rightarrow \Lambda^* \ell^+ \ell^-$ decay in nonuniversal Z' model*, *Int. J. Mod. Phys. A* **37** (2022), no. 09 2250044.

[41] Y.-m. Wang, Y. Li, and C.-D. Lu, *Rare Decays of $\Lambda_b \rightarrow \Lambda + \gamma$ and $\Lambda_b \rightarrow \Lambda + l^+ l^-$ in the Light-cone Sum Rules*, *Eur. Phys. J. C* **59** (2009) 861–882, [[arXiv:0804.0648](https://arxiv.org/abs/0804.0648)].

[42] Y.-M. Wang, Y.-L. Shen, and C.-D. Lu, $\Lambda_b \rightarrow p, \Lambda$ transition form factors from QCD light-cone sum rules, *Phys. Rev. D* **80** (2009) 074012, [[arXiv:0907.4008](https://arxiv.org/abs/0907.4008)].

[43] A. Khodjamirian, C. Klein, T. Mannel, and Y. M. Wang, *Form Factors and Strong Couplings of Heavy Baryons from QCD Light-Cone Sum Rules*, *JHEP* **09** (2011) 106, [[arXiv:1108.2971](https://arxiv.org/abs/1108.2971)].

[44] T. Mannel and Y.-M. Wang, *Heavy-to-light baryonic form factors at large recoil*, *JHEP* **12** (2011) 067, [[arXiv:1111.1849](https://arxiv.org/abs/1111.1849)].

[45] L.-F. Gan, Y.-L. Liu, W.-B. Chen, and M.-Q. Huang, *Improved Light-cone QCD Sum Rule Analysis Of The Rare Decays $\Lambda_b \rightarrow \Lambda \gamma$ And $\Lambda_b \rightarrow \Lambda l^+ l^-$* , *Commun. Theor. Phys.* **58** (2012) 872–882, [[arXiv:1212.4671](https://arxiv.org/abs/1212.4671)].

[46] Y.-M. Wang and Y.-L. Shen, *Perturbative Corrections to $\Lambda_b \rightarrow \Lambda$ Form Factors from QCD Light-Cone Sum Rules*, *JHEP* **02** (2016) 179, [[arXiv:1511.09036](https://arxiv.org/abs/1511.09036)].

[47] K.-S. Huang, H.-Y. Jiang, and F.-S. Yu, *Transition form factors of the $\Lambda_b \rightarrow \Lambda(1520)$ in QCD light-cone sum rules*, *Eur. Phys. J. C* **85** (2025), no. 3 351, [[arXiv:2412.06515](https://arxiv.org/abs/2412.06515)].

[48] T. M. Aliev, T. Barakat, and M. Savci, *Form factors for the rare $\Lambda_b(\Lambda_b^*) \rightarrow N \ell^+ \ell^-$ decays in light cone QCD sum rules*, *Phys. Rev. D* **98** (2018), no. 3 035033, [[arXiv:1807.04101](https://arxiv.org/abs/1807.04101)].

[49] B. L. Ioffe, *Calculation of Baryon Masses in Quantum Chromodynamics*, *Nucl. Phys. B* **188** (1981) 317–341. [Erratum: *Nucl.Phys.B* 191, 591–592 (1981)].

[50] E. V. Shuryak, *Hadrons Containing a Heavy Quark and QCD Sum Rules*, *Nucl. Phys. B* **198** (1982) 83–101.

[51] Y. Chung, H. G. Dosch, M. Kremer, and D. Schall, *Baryon Sum Rules and Chiral Symmetry Breaking*, *Nucl. Phys. B* **197** (1982) 55–75.

[52] **Particle Data Group** Collaboration, S. Navas et al., *Review of particle physics*, *Phys. Rev. D* **110** (2024), no. 3 030001.

[53] Y.-L. Liu and M.-Q. Huang, *Distribution amplitudes of Sigma and Lambda and their electromagnetic form factors*, *Nucl. Phys. A* **821** (2009) 80–105, [[arXiv:0811.1812](https://arxiv.org/abs/0811.1812)].

[54] K. G. Chetyrkin, J. H. Kuhn, A. Maier, P. Maierhofer, P. Marquard, M. Steinhauser, and C. Sturm, *Charm and Bottom Quark Masses: An Update*, *Phys. Rev. D* **80** (2009) 074010, [[arXiv:0907.2110](https://arxiv.org/abs/0907.2110)].

[55] T. Feldmann and M. W. Y. Yip, *Form factors for $\Lambda_b \rightarrow \Lambda$ transitions in the soft-collinear effective theory*, *Phys. Rev. D* **85** (2012) 014035, [[arXiv:1111.1844](https://arxiv.org/abs/1111.1844)]. [Erratum: *Phys. Rev. D* 86, 079901 (2012)].

[56] W. Detmold and S. Meinel, *$\Lambda_b \rightarrow \Lambda \ell^+ \ell^-$ form factors, differential branching fraction, and angular observables from lattice QCD with relativistic b quarks*, *Phys. Rev. D* **93** (2016), no. 7 074501, [[arXiv:1602.01399](https://arxiv.org/abs/1602.01399)].

[57] C. Bourrely, I. Caprini, and L. Lellouch, *Model-independent description of $B \rightarrow \pi \ell \nu$ decays and a determination of $|V_{ub}|$* , *Phys. Rev. D* **79** (2009) 013008, [[arXiv:0807.2722](https://arxiv.org/abs/0807.2722)]. [Erratum: *Phys. Rev. D* 82, 099902 (2010)].

[58] F. Mahmoudi, *SuperIso: A Program for calculating the isospin asymmetry of $B \rightarrow K^* \gamma$ in the MSSM*, *Comput. Phys. Commun.* **178** (2008) 745–754, [[arXiv:0710.2067](https://arxiv.org/abs/0710.2067)].

[59] F. Mahmoudi, *SuperIso v2.3: A Program for calculating flavor physics observables in Supersymmetry*, *Comput. Phys. Commun.* **180** (2009) 1579–1613, [[arXiv:0808.3144](https://arxiv.org/abs/0808.3144)].

[60] S. Neshatpour and F. Mahmoudi, *Flavour Physics with SuperIso*, *PoS TOOLS2020* (2021) 036, [[arXiv:2105.03428](https://arxiv.org/abs/2105.03428)].